Berichte
zur Polar- und Meeresforschung

655
2012

Reports on Polar and Marine Research

Expeditions to Permafrost 2012:
"Alaskan North Slope / Itkillik",
"Thermokarst in Central Yakutia",
"EyeSight-NAAT-Alaska"

Edited by
Jens Strauss, Mathias Ulrich and Marcel Buchhorn
with contributions of the participants

HELMHOLTZ GEMEINSCHAFT

ALFRED-WEGENER-INSTITUT FÜR
POLAR- UND MEERESFORSCHUNG
in der Helmholtz-Gemeinschaft
D-27570 BREMERHAVEN
Bundesrepublik Deutschland

ISSN 1866-3192

Hinweis

Die Berichte zur Polar- und Meeresforschung werden vom Alfred-Wegener-Institut für Polar- und Meeresforschung in Bremerhaven* in unregelmäßiger Abfolge herausgegeben.

Sie enthalten Beschreibungen und Ergebnisse der vom Institut (AWI) oder mit seiner Unterstützung durchgeführten Forschungsarbeiten in den Polargebieten und in den Meeren.

Es werden veröffentlicht:

— Expeditionsberichte (inkl. Stationslisten und Routenkarten)

— Expeditions- und Forschungsergebnisse (inkl. Dissertationen)

— wissenschaftliche Berichte der Forschungsstationen des AWI

— Berichte wissenschaftlicher Tagungen

Die Beiträge geben nicht notwendigerweise die Auffassung des Instituts wieder.

Notice

The Reports on Polar and Marine Research are issued by the Alfred Wegener Institute for Polar and Marine Research in Bremerhaven*, Federal Republic of Germany. They are published in irregular intervals.

They contain descriptions and results of investigations in polar regions and in the seas either conducted by the Institute (AWI) or with its support.

The following items are published:

— expedition reports (incl. station lists and route maps)

— expedition and research results (incl. Ph.D. theses)

— scientific reports of research stations operated by the AWI

— reports on scientific meetings

The papers contained in the Reports do not necessarily reflect the opinion of the Institute.

The „Berichte zur Polar- und Meeresforschung” continue the former „Berichte zur Polarforschung”

* Anschrift / Address
Alfred-Wegener-Institut
für Polar- und Meeresforschung
D-27570 Bremerhaven
Germany
www.awi.de

Editor:
Dr. Horst Bornemann

Assistant editor:
Birgit Chiaventone

Die "Berichte zur Polar- und Meeresforschung" (ISSN 1866-3192) werden ab 2008 als Open-Access-Publikation herausgegeben (URL: http://epic.awi.de).

Since 2008 the "Reports on Polar and Marine Research" (ISSN 1866-3192) are available as open-access publications (URL: http://epic.awi.de)

Expeditions to Permafrost 2012:
"Alaskan North Slope / Itkillik",
"Thermokarst in Central Yakutia",
"EyeSight-NAAT-Alaska"

Edited by
Jens Strauss, Mathias Ulrich and Marcel Buchhorn
with contributions of the participants

Please cite or link this publication using the identifier
hdl: 10013/epic.40371 or http://hdl.handle.net/10013/epic.40371

ISSN 1866-3192

German expedition leaders / principal investigators:

Alaskan North Slope / Itkillik:

Jens Strauss
Alfred Wegener Institute for Polar and Marine Research
Department of Periglacial Research
Telegrafenberg A45, 14473 Potsdam, Germany

Thermokarst in Central Yakutia

Dr. Mathias UIrich
Alfred Wegener Institute for Polar and Marine Research
Department of Periglacial Research
Telegrafenberg A45, 14473 Potsdam, Germany
Current address
University of Leipzig, Institute for Geography
Johannisallee 19a, 04103 Leipzig, Germany

EyeSight-NAAT Alaska

Marcel Buchhorn
Alfred Wegener Institute for Polar and Marine Research
Department of Periglacial Research
Telegrafenberg A5, 14473 Potsdam, Germany

International expedition leaders / principal investigators:

Alaskan North Slope / Itkillik:

Prof. Dr. Yuri Shur and Dr. Mikhail Kanevskiy
University of Alaska Fairbanks, Institute of Northern Engineering
539 Duckering Building, 306 Tanana Loop
Fairbanks, Alaska 99775, United States of America

Thermokarst in Central Yakutia

Dr. Alexander Fedorov
Melnikov Permafrost Institute SB RAS
36 Merzlotnaya Str., 677010 Yakutsk, Russia

CONTENT

1. EXPEDITION ALASKAN NORTH SLOPE / ITKILLIK 2012

Jens Strauss, Yuri Shur, Mikhail Kanevskiy, Daniel Fortier, Kevin Bjella, Amy Breen and Cody Johnson

1.1. Introduction

Scientific Rationale and Objectives

Fieldwork on the Alaskan North Slope of the Brooks Range at the Itkillik River exposure was undertaken by an international team with participants from the United States of America, Canada, Russia, and Germany in spring 2012.

The overall aim of the study was to investigate the dynamics and consequences of increasing permafrost degradation as well as quality and quantity of organic matter (OM) stored in Alaskan late Pleistocene syngenetic permafrost deposits (Yedoma). These sediments are very ice rich and contain very large ice wedges. Kanevskiy et al. [2011] and Schirrmeister et al. [in press] give a review of the Yedoma definitions in Russia and North America. Compared to Siberian Yedoma, the Alaskan organic- and ice-rich deposits are insufficiently studied. In the context of global warming, thawing of this extremely ice-rich material can significantly alter the landscape, in particular with respect to ground subsidence. The total thaw settlement of the Itkillik Yedoma can reach at least 20 m, which corresponds to observed depths of thaw-lake basins in the study area [Kanevskiy et al. 2011]. In this case, the OM can be remobilized and reintroduced into the recent carbon cycle by thermal destabilization. Data of the characteristics and quantity of the ground ice and OM in the frozen sediments of the Itkillik River exposure will improve the understanding of the climatic or anthropogenic driven response of this sensitive component of the Arctic geosystem.

Methodically, it is planned to analyze the Yedoma sediments and the OM using lipid biomarkers. Thus, the sediment accumulation and the transformation of the OM during earlier climatic cycles will be studied.

The expedition Alaskan North Slope / Itkillik 2012 was focused on combined studies of permafrost sequences using the exposed bluff and boreholes from the Yedoma top. Expected results of cryolithological and stratigraphical studies will be used as a reference for comparison and correlation with results of similar studies of permafrost sequences in Siberia and Alaska. An interdisciplinary sampling approach that combined the fields of sedimentology, geocryology, and biogeochemistry was applied. The topics of the fieldwork in May 2012 were the following:

- Ice wedge degradation
- Modern cryosoils
- Geocryolithology
- Cryostratigraphy
- Geochronology
- Biogeochemistry
- Paleoecology

Expedition Itinerary and General Logistics

Seven participants from the University of Alaska Fairbanks (UAF), the United States Army Cold Regions Research and Engineering Laboratory (CRREL), CH2M HILL Polar Service and the Alfred Wegener Institute for Polar and Marine Research (AWI Potsdam) took part in the field work (Fig. 1.1 and Tab. 1.1).

Fig. 1.1: *Participants from left to right: Amy Breen (UAF), Cody Johnson (CH2M HILL Polar Service), Kevin Bjella (CRREL), Mikhail Kanevskiy (UAF), Yuri Shur (UAF), Daniel Fortier (Université de Montréal) and Jens Strauss (AWI)*

To access the field site, the participants drove with two Ford F350 trucks from Fairbanks to Toolik Field Station, a UAF scientific research station north of the Brooks Range (Fig. 1.2a). At Toolik they stayed for one night. The following day the participants flew to the Itkillik field site. From Galbraith Lake airstrip, ~15 km south of Toolik, a fixed wing single engine DeHavilland Beaver, (Fig. 1.2b) operated by Coyote Air, was used. Because of retractable skis capable of wheel landing at the Galbraith Lake airstrip and ski landing on the snow at the field site, the Beaver aircraft had ideal characteristics for this expedition.

a **b**

Fig. 1.2: *Vehicles used to reach the Itkillik field site. Pictures by J. Strauss*

Tab. 1.1: *Participants of the expedition Alaskan North Slope / Itkillik 2012, list of participants is sorted alphabetically.*

Participant	Organisation/Institute	E-mail
Bjella, Kevin	U.S. Army Cold Regions Research and Engineering Laboratory (CRREL)	Kevin.Bjella@usace.army.mil
Breen, Amy	University of Alaska Fairbanks (UAF)	albreen@alaska.edu
Fortier, Daniel	Université de Montréal	Daniel.Fortier@umontreal.ca
Johnson, Cody	CH2M HILL Polar Service	Cody@polarfield.com
Kanevskiy, Mikhail (co-Principle investigator)	University of Alaska Fairbanks (UAF)	mkanevskiy@alaska.edu
Shur, Yuri (Principle investigator)	University of Alaska Fairbanks (UAF)	yshur@alaska.edu
Strauss, Jens	Alfred-Wegener-Institute	Jens.Strauss@awi.de

The expedition itinerary is shown in Tab. 1.2. The fieldwork was completed on May 14th and that evening two shuttle flights with 5 participants and field gear flew back to Toolik. Because of poor weather conditions, the last two shuttle flights were shifted to the next day. On May 16, the participants drove back to Fairbanks.

Tab. 1.2: *Time table for the expedition Alaskan North Slope / Itkillik 2012*

Date	Location	Task
07.05.2012	Fairbanks	Preparation of the trucks
08.05.2012	Fairbanks and Toolik Field Station	Departure from Fairbanks to Toolik Field Station with two trucks via Elliot and Dalton Highway
09.05.2012	Toolik Field Station and Itkillik River exposure	Transport from Toolik Field Station to Gailbraith Lake. Three flights from airstrip at Gailbraith Lake to Itkillik River exposure
10.-14.05.2012	Itkillik River exposure	Field work
14.05.2012	Itkillik River exposure and Toolik Field Station	Two flights from Itkillik River exposure to airstrip at Galbraith Lake and transport to Toolik Field Station
15.05.2012	Itkillik River exposure and Toolik Field Station	Two flights from Itkillik River exposure to airstrip at Galbraith Lake and transport to Toolik Field Station
16.05.2012	Toolik Field Station and Fairbanks	Departure from Toolik Field Station to Fairbanks with two trucks via Dalton and Elliot Highway

1.2. Itkillik Permafrost Sequence

Study Site and Geomorphological Description of the Area

The study area is situated at the right bank of the Itkillik River (69°34′ N, 150°52′ W) at the boundary between the Arctic Coastal Plain and the Arctic Foothills (Fig. 1.3 and Fig. 1.4). The ice-rich silts of the Itkillik bluff are exposed in a ~400 m long bluff cutting a Yedoma hill (Fig. 1.5, Fig. 1.6 and Fig. 1.7) [Kanevskiy et al. 2011]. The hill surface is a relict part of a former Yedoma plain and its elevation is about 30 to 35 m above the Itkillik River water level (Fig. 1.7). Kanevskiy et al. [2011] first described the Itkillik River exposure. In the appendix chapter A.1 data from previous studies are described.

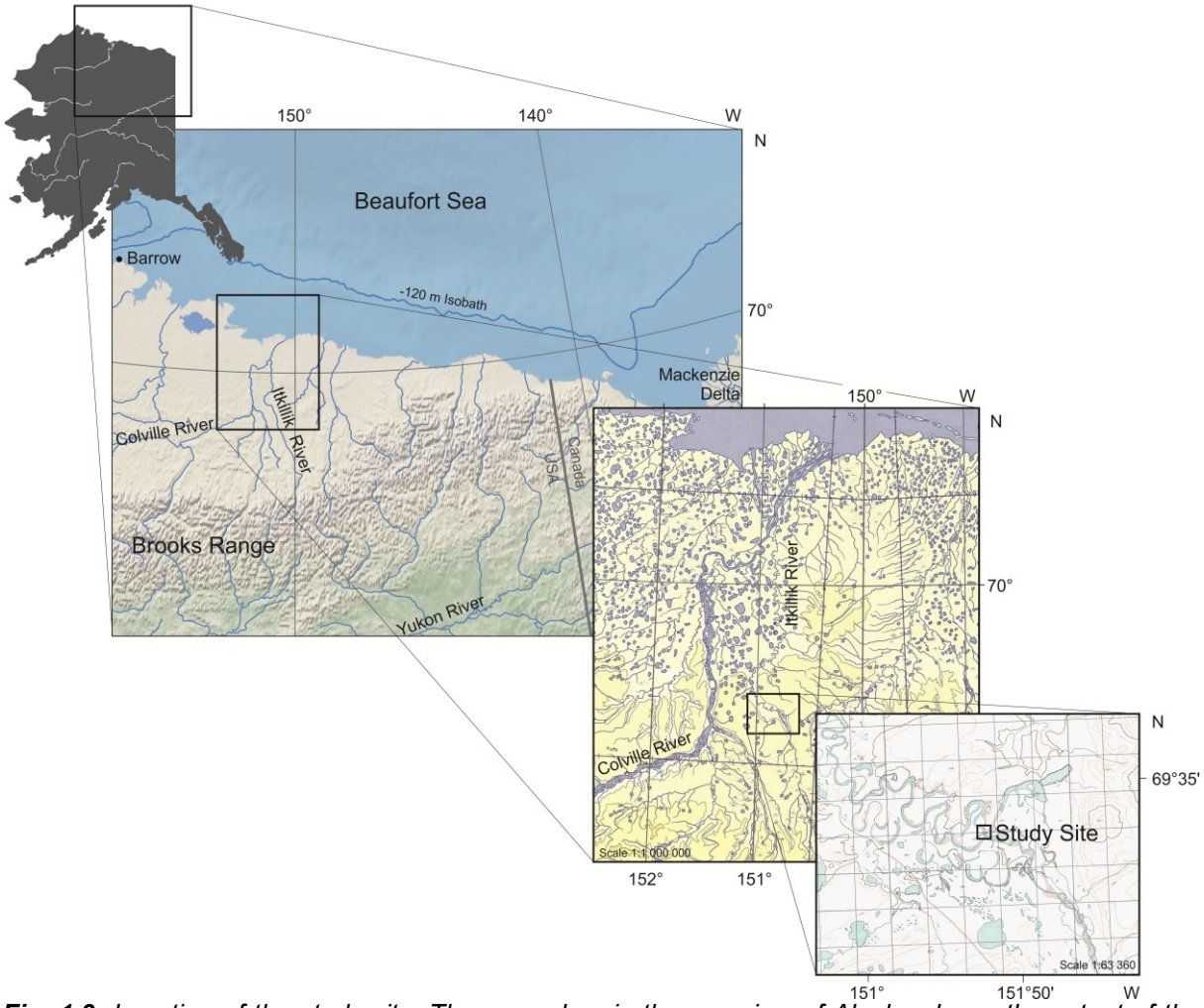

Fig. 1.3: *Location of the study site. The upper box in the overview of Alaska shows the extent of the map below. The detailed topographic map (scale 1:63 360) is compiled by USGS in 1971.*

In addition, Carter [1988] published a description of two exposures north of the study site. The exposure sampled during this expedition, as well as Carters [1988] sites 2 and 3, are part of the same remnant of a continuous Yedoma plain [Kanevskiy et al. 2011].

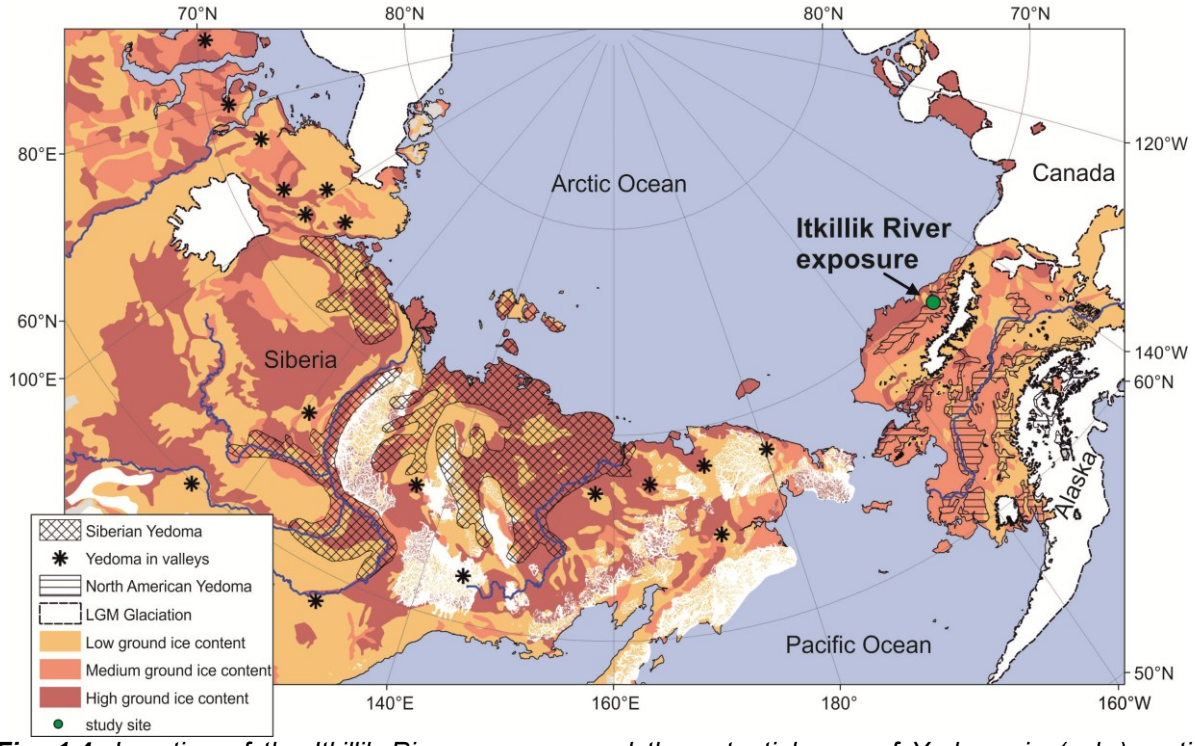

Fig. 1.4: *Location of the Itkillik River exposure and the potential area of Yedoma in (sub-) arctic lowlands of late Pleistocene Beringia. Map published in Strauss et al. [2012], based on Romanovskii [1993] for Siberian Yedoma, Péwé [1975] and Wolfe et al. [2009] for North American Yedoma, Ehlers and Gibbard [2003] for last glacial maximum glaciation, and Brown et al. [1997] for ground-ice content. From Strauss et al. [2012], modified after a map compiled by G. Grosse (University of Alaska Fairbanks).*

The bluff is eroded by a meander of the Itkillik River (Fig. 1.5, Fig. 1.6 and Fig. 1.7). On the eastern part, behind the exposure wall, a crack (up to 2m wide, Fig. 1.5 and Fig. 1.8) was observed. Likely, this crack will cause block-failure of a portion of the Yedoma shortly. At this part of the exposure the Itkillik River erodes a thermo-erosional niche at the base (Fig. 1.6, Fig. 1.7 and Fig. 1.9) and destabilizes the exposure, which may have caused the crack. Approximately 1 km north of the exposure a pingo (Fig. 1.10) is located.

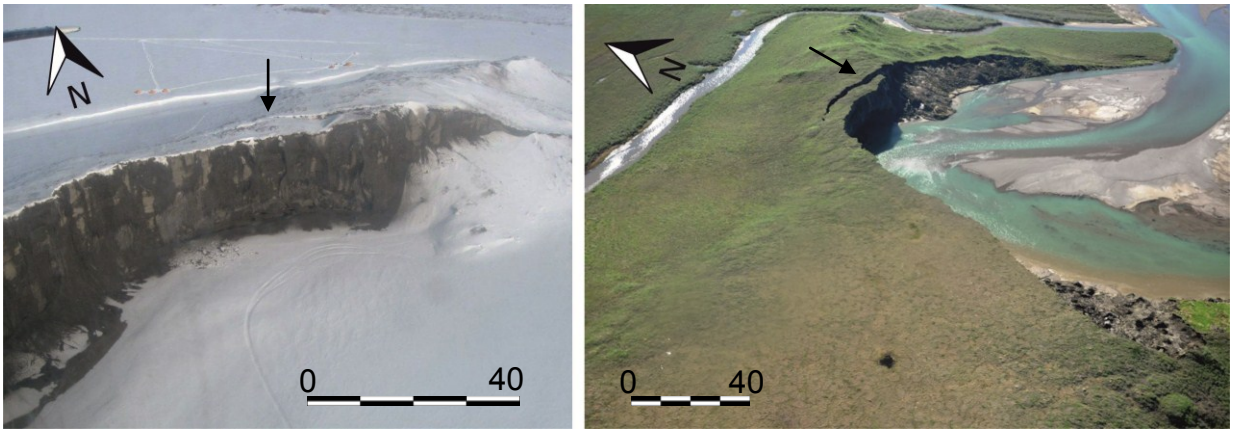

Fig. 1.5: *Aerial view on Itkillik River exposure during spring (left) and summer (right) 2012. The arrows on both pictures mark a crack at the eastern part of the bluff. Scale in meter. Pictures from K. Bjella (left, May 2012) and A. Breen (right, June 2012)*

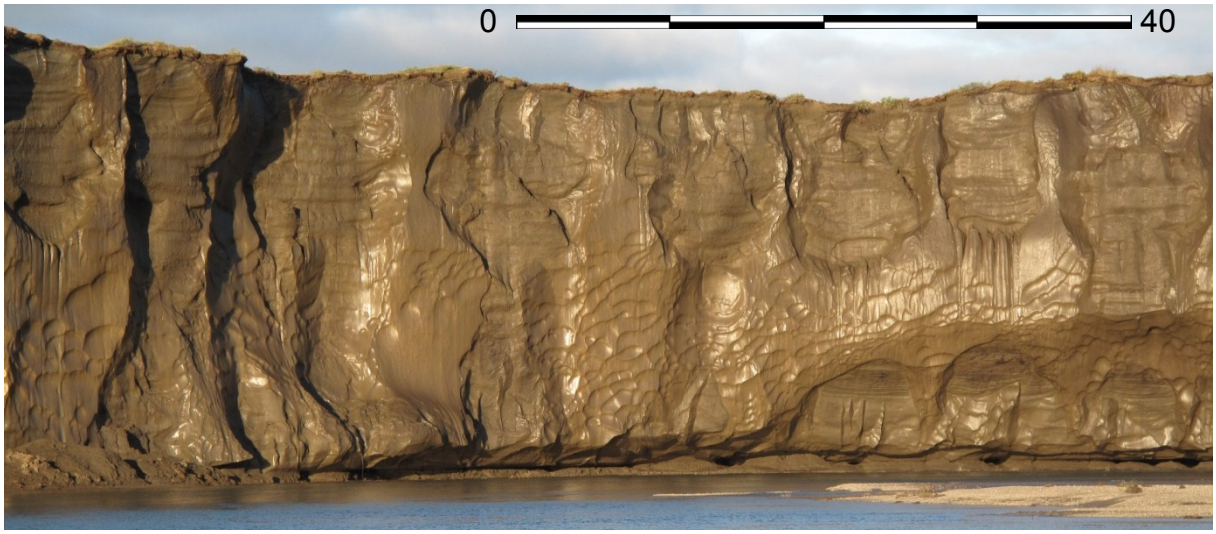

Fig. 1.6: *Itkillik exposure during summer 2011. Scale in meter. Picture by M. Kanevskiy (August 2011)*

In general, the exposed deposits do not have distinct stratification. However, there are pseudo-stratifications visible, mostly of cryogenic origin: it is formed by ice belts (showing former positions of permafrost table during the periods of slower Yedoma accumulation) and layers with different cryostructures. So these deposits are sub-horizontally stratified, as evidenced by horizontal thawing and freezing at the lower active layer boundary. Visible organic matter is sparse, but present throughout the whole profile as rootlets or rarely macro-plant remains like woody stems and twigs less than 1 cm in diameter.
The ice wedges have shoulders at several depths, which is characteristic for syngenetic growth. Depending on their position in the profile, the apparent width of the ice wedges was >6 m at the lower part (30 to >~13 meters below surface level; m b.s.l.) and > 3 m at the upper part (<~13 m b.s.l.).

Field Methods and Sampling Strategy

After a reconnaissance trip, a sediment column between two ice wedges in the central part of the exposure was selected for detailed studies and sampling (Fig. 1.7, part It and Itk-C & D). For sampling also the upper part of the sediments and the ice wedge, anchors for rapelling down from the top of the bluff (Fig. 1.11) were installed.
One major sequence (Itk-C, Itk-D and It) and several smaller separate profiles below (Itk-B) or sideways from the major sequence (Itk-E, Itk-F, Itk-G, Itk-H, Itk-I, Itk-J) were sampled to maximize the record of Yedoma deposits. It was necessary to sample beside the major profile because of an overhang between 20.5 to 9.7 m b.s.l. as it was impossible to reach the bluff wall there. Therefore, accessible sampling points and conical thermokarst mounds (baidzharakhs as an intact remnant of a former sediment column between ice wedge) were used to fill these gaps. The correlation of the sampling positions was done by height estimation using measuring tape. The sampling depth beside the main profile was calibrated with tacheometer measurements and a level instrument. For geochronological and stratigraphical interpretation it is planned to date several samples and stack them together to comprise a composite profile. The chosen sequences were surveyed, described, photographed, and sketched according to sediment- and cryostructures.

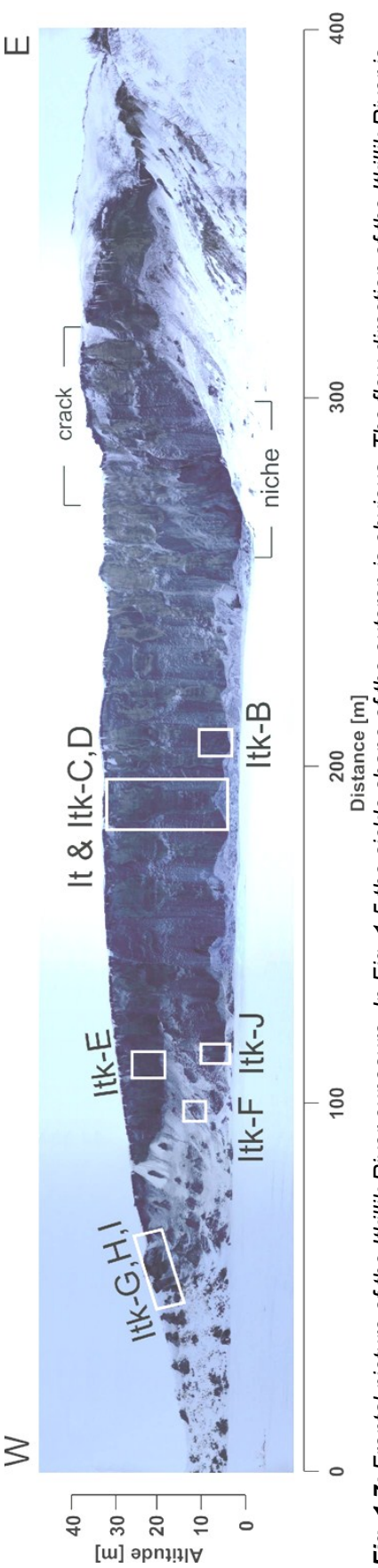

Fig. 1.7: *Frontal picture of the Itkillik River exposure. In Fig. 1.5 the sickle shape of the outcrop is obvious. The flow direction of the Itkillik River is from east to west. Merged pictures by J. Strauss, May 2012*

Fig. 1.8: *Photograph of the crack. Picture by D. Fortier.*

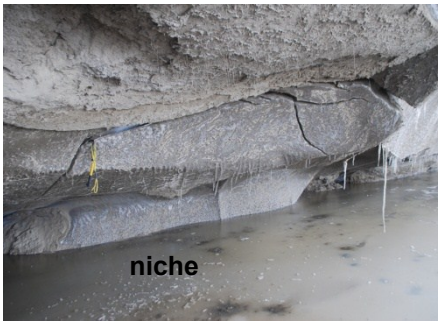

Fig. 1.9: *Niche formed by Itkillik River erosion. Pickaxe (left) for scale. Picture by D. Fortier.*

Fig. 1.10: *Picture from the top of the Yedoma hill in northern direction to the Pingo. Picture by J. Strauss.*

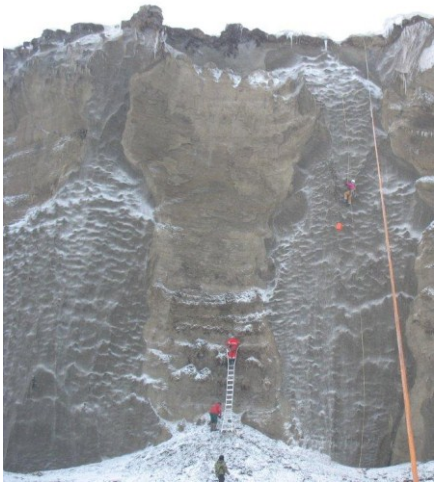

Fig. 1.11: *Sampling sediment column and ice wedge. Picture by C. Johnson.*

Before sampling, frozen deposits were cleaned with a hammer, a pick or an axe. Three subsamples were taken for further multidisciplinary studies (sedimentology, paleoecology, geochronology, biogeochemistry) using a hand held electric drill and a core-drill of 4.7 cm in diameter.
At each stratigraphic location, two sediment samples were packed in plastic bags and one sediment sample (for lipid biomarker measurements) was packed in pre-burned sterile glassware. For all sediment samples, the drilling mud was removed.
The sample name code for the majority of the sediment samples is composed of:

- study area: Itk for Itkillik
- a letter for each sub-profile: e.g. Itk-B
- the sample number: e.g. Itk-B-02

For ice/water-content and bulk-density calculation in the field laboratory one set of subsamples packed in plastic bags was weighed using a balance (Kern FCB 8K0.1). As a second step, the sample volume was determined using the displacement in a beaker glass filled with water (Archimedes Principle).
All samples were kept frozen in a cooler buried in snow during the fieldwork period. For transportation and shipping, dry ice was used. Detailed photographs and profile schemes of the sampled sites are supplemented in the following chapters of this report. The legend for these figures is given in Fig. 1.12.

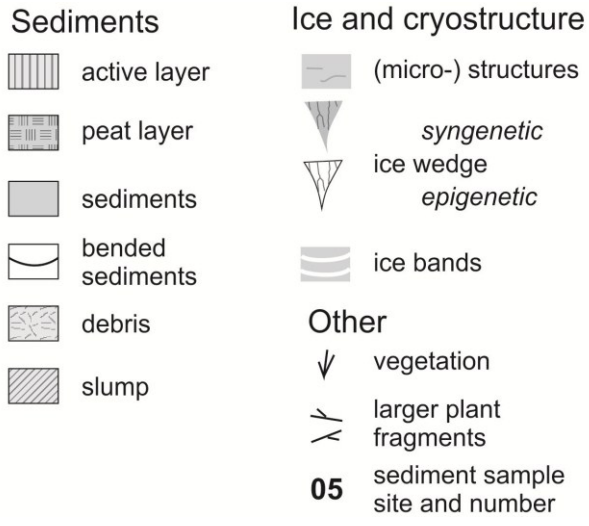

Fig. 1.12: *Legend of the signatures used in the sub-profile schemes Fig. 1.15, Fig. 1.16, Fig. 1.19b, Fig. 1.20, Fig. 1.21b.*

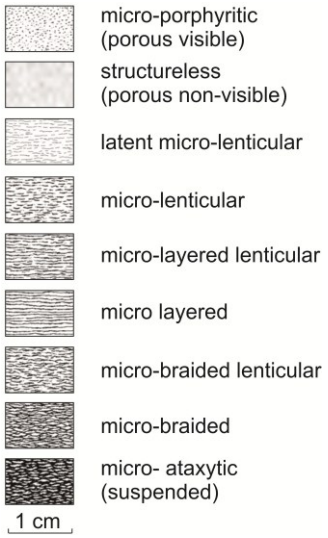

Fig. 1.13: *Micro-cryostructures typical of syngenetic permafrost (ice: black), The terms are used for cryolithological descriptions. Figure modified from Kanevskiy et al. [2011].*

Cryolithological Description in the Laboratory

Immediately after returning to Fairbanks, the cryostructures were described in detail. Therefore, one subset of samples was cleaned and prepared in a cold room for taking high quality pictures. Different cryostructures according to French and Shur [2010] and Kanevskiy et al. [2011] (Fig. 1.13) were observed. Fig. 1.14 shows selected examples of identified cryostructures. Sample It-1 (Fig. 1.14a) is identified as micro-braided. The results of the cryostructural descriptions are integrated in the description of the sampled profiles below.

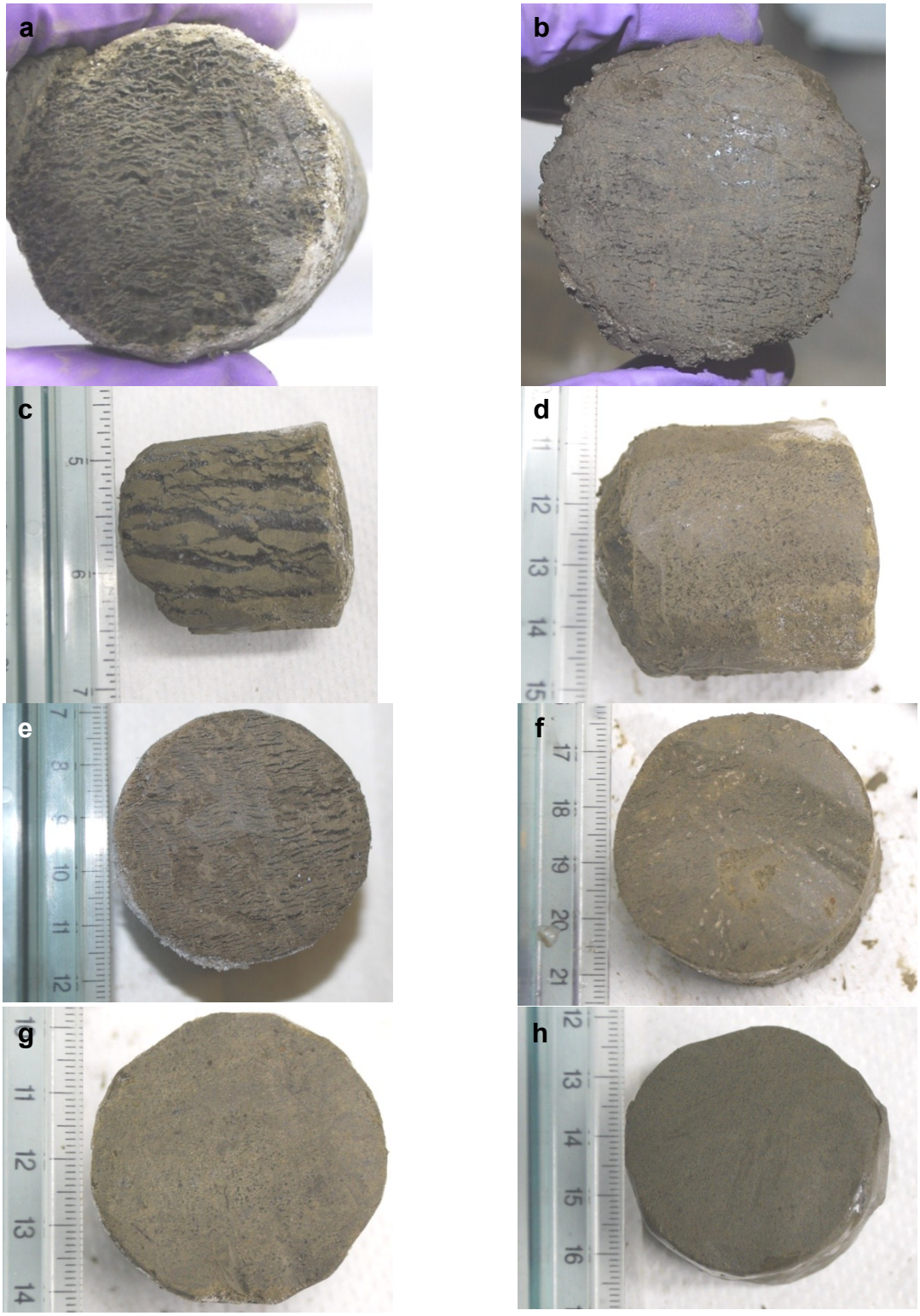

Fig. 1.14: *Pictures of the sediment samples and their cryostructure; a) It-1 (2.1 m b.s.l.), micro-braided to micro-ataxitic cryostructure; b) Itk-B-02 (27.5 m b.s.l.), micro-lenticular to micro-braided cryostructure; c) Itk-D-03 (24.8 m b.s.l.), braided to ataxitic (suspended) cryostructure; d) Itk-E-03 (9.2 m b.s.l.), latent micro-lenticular cryostructure to porous visible, e) Itk-F-02 (20.2 m b.s.l.), latent micro-lenticular; f) Itk-G-02 (15.9 m b.s.l.), micro-lenticular to micro-braided cryostructure; g) Itk-I-02 (10.6 m b.s.l.), micro-porphyritic cryostructure; h) Itk-J-02 (28.9 m b.s.l.), structureless cryostructure. All pictures by D. Fortier (May 2012)*

Sampled Permafrost Profiles

For this report, the sampled sub-profiles are sorted in a stratigraphical order from bottom to top as far as possible. Fig. 1.7 gives an orientation where the sub-profiles are located.

Sub-profile Profile Itk-J

The lowermost sub-profile Itk-J (29.8 to 28.3 m. b.s.l., Fig. 1.15) is located ca 60 m left of the major profile.
The sediment is composed of (gray-) brownish silt, like the majority of the samples from the Itkillik River exposure. Macro-plant remains including rootlets are obvious in Itk-J. At this sub profile, the cryostructure is latent micro-lenticular. The sediments are framed by huge syngenetic ice wedges. These ice wedges are composed of numerous separate pure ice veins and ice veins with numerous soil particles concentrated along the vein axes. The ice is clear to yellowish, rarely including gas bubbles.

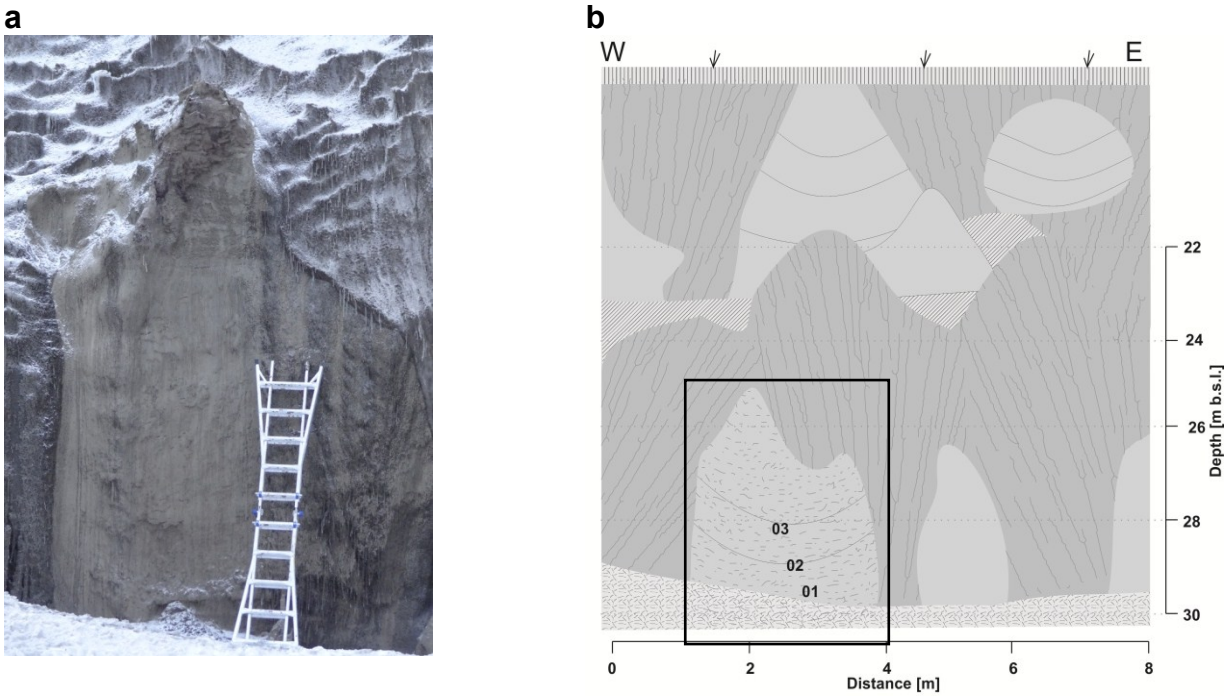

Fig. 1.15: *a) Picture and b) schematic of sub-profile Itk-J; the box in b marks the extent of the photograph a. The scale in b is based on the front schematic and is not usable for the background. Picture by J. Strauss (May 2012).*

The Major Profile Itk-B, Itk-C, Itk-D and It

One long sequence of continuous Yedoma deposits was studied (Fig. 1.16 and Fig. 1.17). The studied ~30 m long sequence reaches from the Itkillik River level, where older permafrost deposits are already buried by debris, up to the upper edge of the exposure. This major profile consists of 4 partly overlapping sub-profiles (Itk-B, Itk-C, Itk-D and It) and 3 samples without a sub-profile classification (14C-1 (20.6 m b.s.l.), Sample 1 and 2 (20.8 to 22.3 m b.s.l.)). The sediment column is framed by two syngenetic ice wedges, which extend from the very top to the bottom of the4 exposure and beyond. The ice wedges are exposed nearly normal to their

orientationand are clearly wedge shaped. At the upper part (~13 to 0 m b.s.l.) the ice wedges width is max. 3 m, in the lower part (bottom to >~13 m b.s.l.) the ice wedges can exceed a width of max ~6 m. The ice wedge is composed of separate ice veins with sometimes soil particles concentrated along the vein axes. The ice is clear including sparsely distributed gas bubbles. The ice wedge on the left side of the major profiles was sampled vertically (Fig. 1.16, 27.8 to 2.3 m b.s.l., 14 vertical samples) and horizontally at 26.8 m b.s.l. every 25 cm (0 to 5.60 m, totally 23 horizontal samples). The lowermost sub-profile Itk-B (28.0 to 26.5 m b.s.l.) is located on the right side of the major profile (Fig. 1.16). It is surrounded by huge syngenetic ice wedges, which is cut slightly diagonal. The sediments are composed of brownish silty material. The cryostructure is micro-lenticular (Fig. 1.14b) with ice lenses orientated in layers. There are just a few visible organic inclusions and plant remains. The sub-profile Itk-C (26.4 to 25.1 m b.s.l.), is situated at the very right side of the soil column close to the ice wedge boundary (Fig. 1.16). At this site, the debris did not cover the very bottom of the bluff. Like Itk-B, Itk-C is characterized by brownish silty deposits with sparsely included plant remains and a (micro-) lenticular cryostructure. At the upper part of Itk-C ice bands are visible (Fig. 1.18c).

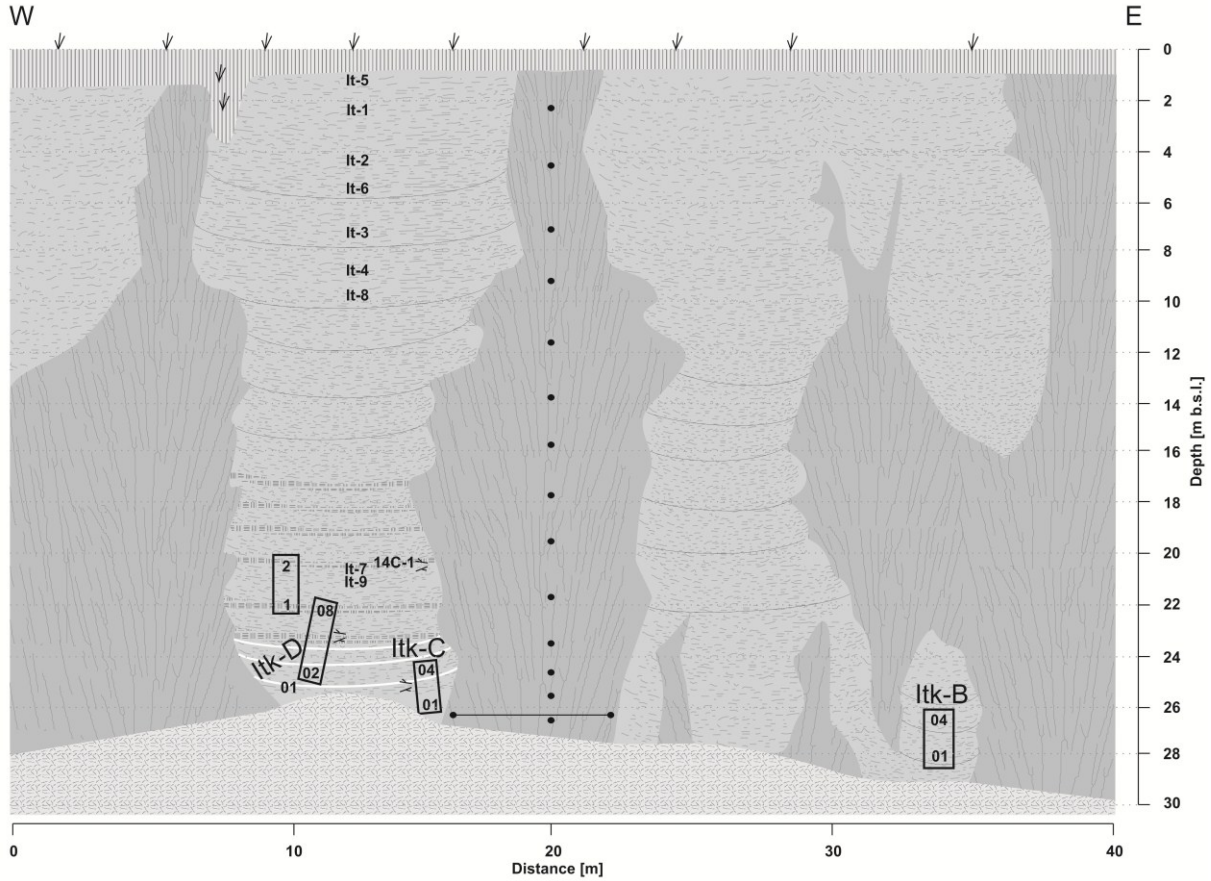

Fig. 1.16: *schematic of the major profile with position of the sub-profiles (Itk-B, Itk-C, Itk-D and It) and sample sites). A picture of this sequence is shown in Fig. 1.17.*

In Itk-D (25.7 to 22.5 m b.s.l., Fig. 1.18c) the same ice bands of Itk-C are continued. The sediments between the ice bands have a lenticular cryostructure, but at the samples Itk-D-03 (Fig. 1.14c) and -07 the cryostructure is banded to ataxitic (suspended). Fig. 1.18c shows an ice band close to sampling point Itk-D-5. The

sediment in Itk-D is silty brownish and at D-05 it is darker with more organic matter inclusions. Sample Itk-D-08 (22.5 m b.s.l.) is a peat layer with slightly decomposed organic matter and macro-plant remains included. Sample 1 and 2 (22.3 and 20.8 m b.s.l.) are composed of brownish sediments. Very close to these sampling points there are peat layers. The cryostructure for Sample 2 is micro-lenticular. Samples It-9 and It-7 have a structureless to micro-lenticular cryostructure. Sample 14C-1 (20.6 m b.s.l.) was taken from one of the peat layers/paleosol horizons. In total, six peat layers were identified at the major profile between 26 and 16 m b.s.l. (Fig. 1.16 and Fig. 1.17).

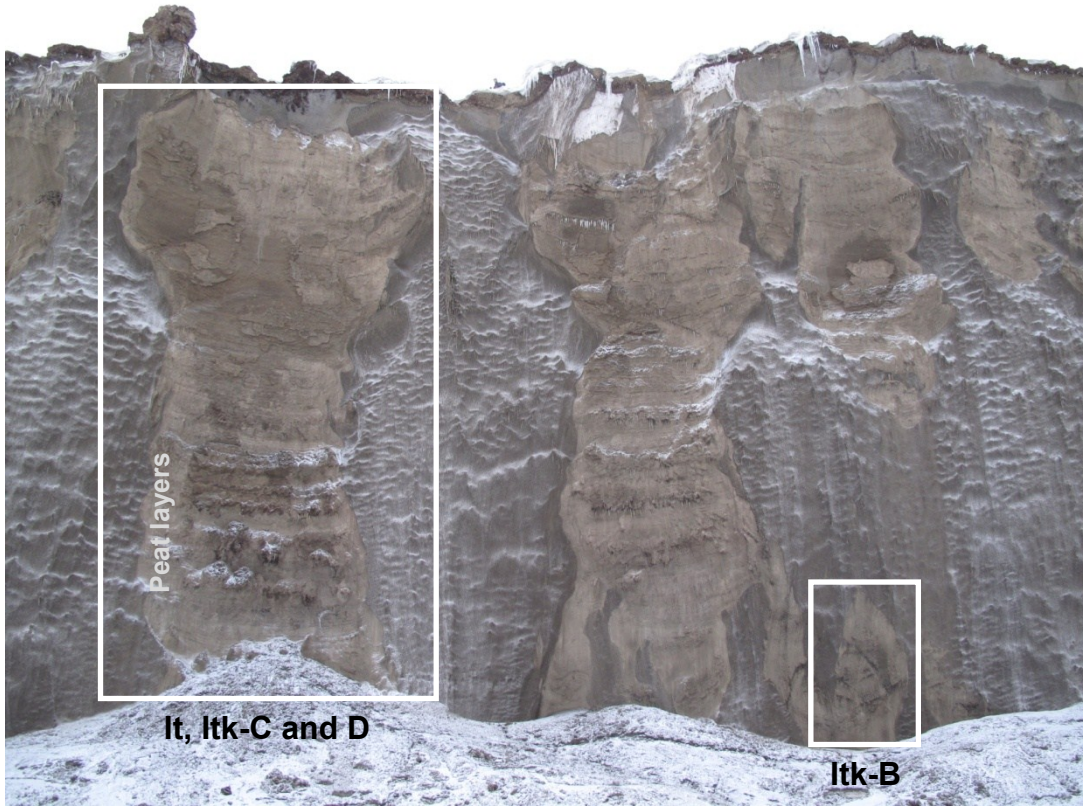

Fig. 1.17: *Overview of the major profile. The sampling areas are identified by white boxes. A schematic of this profile is shown in Fig. 1.16. Picture by J. Strauss (May 2012).*

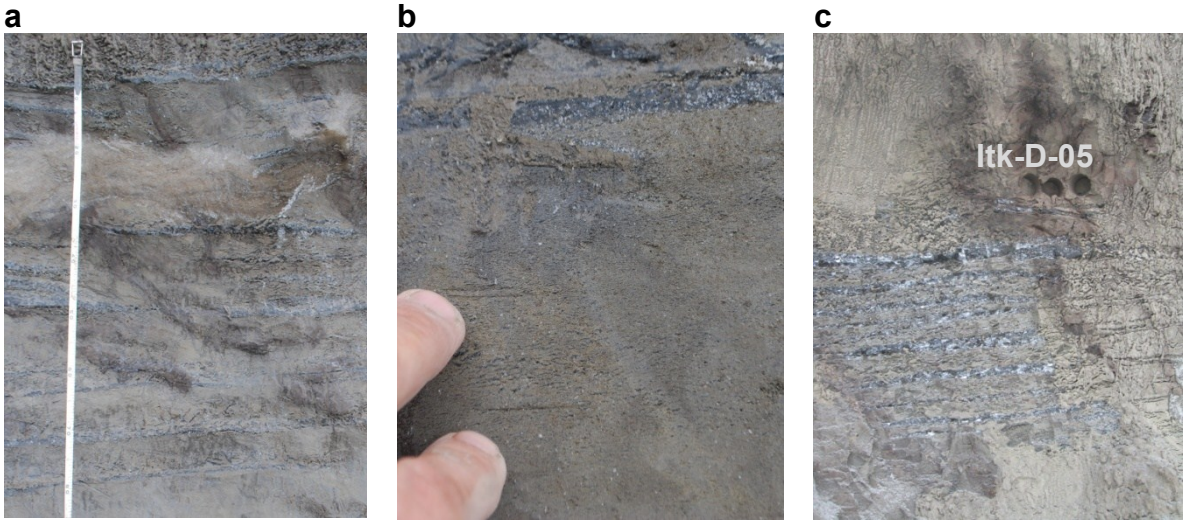

Fig. 1.18: *Cryostructures close to profile Itk-C and Itk-D; picture of a) of ice bands >3 cm and b) ice*

band above lenticular structure. Part c) illustrates the ice bands below sampling point Itk-D-05 (24.0 m b.s.l.). For scale in c, the diameter of one whole is 4.7 cm. Pictures a, b by D. Fortier, c by J. Strauss.

The positions of three lower peat layers were identified using measurement tape. The lowest peat layer is from 24.3 to 23.3 m b.s.l. and the next upper one from 22.7 to 21.5 m b.s.l. At the upper part of the major profile (It-1 to 6 and It-8, 0.5 to 9.7 m b.s.l.) sampling was done using climbing gear by repelling down from the top of the bluff (Fig. 1.11). The sediments are brownish and silty like the samples below. The cryostructure of the part between It-8 to It-2 (9.7 to 4.7 m b.s.l.) is composed of hardly visible micro-cryostructures (porphyritic, latent micro-lenticular) to structureless. The cryostructure at the top (2.3 to 0.5 m b.s.l.) is micro-braided (Fig. 1.14a) to reticulate at the very top (It-5).

Sub-profile Itk-F

The sampled baidzharakh sub-profile Itk-F (21.0 to 19.5, Fig. 1.19) was located below to sub-profile Itk-E.

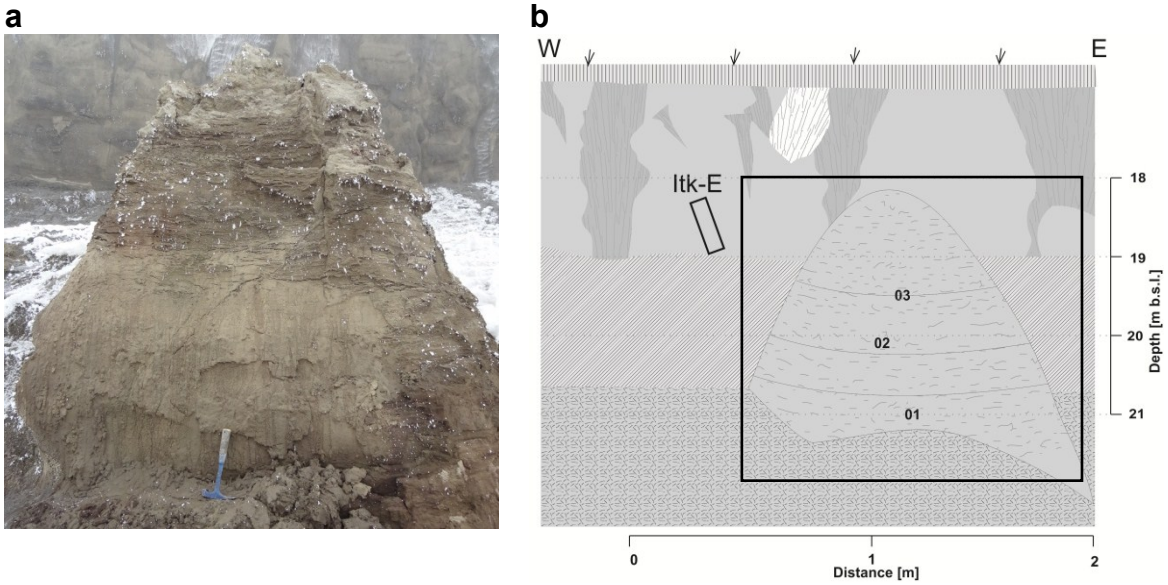

Fig. 1.19: *a) Picture and b) schematic of the baidzharakh containing sub-profile Itk-F; figure b) also shows the relative position of sub-profile Itk-F to sub-profile Itk-E in the background of the baidzharakh. The scale in b is based on the baidzharakh; for the background, like the Itk-E profile, the scale of Fig. 1.21 has to be used. The box in b marks the extent of the photograph in a. Picture by J. Strauss (May 2012).*

The baidzharakh is an intact remnant of a former sediment column between ice wedges, sticks out of a thermoterrace/debris. The sediments are brownish and silty. The cryostructure is micro-lenticular at the bottom of the baidzharakh, (micro-) lenticular at Itk-F-02 (Fig. 1.14e) and structureless at the uppermost sample. Especially at the upper part of this baidzharakh, a sub horizontal stratification is visible, which is permeated by rootlets. Rarely other macro-plant remains are visible.

Sub-profile Itk-G, Itk-H, Itk-I

The sub-profiles Itk-G, Itk-H and Itk-I are ~150 m left of the major profile (Fig. 1.7). The whole bluff is sickle shaped (Fig. 1.5) and at the sampled profiles the bluff is east

facing (Fig. 1.20). The ice wedges between the sub-profiles were partly snow covered. All sediments in the sub-profile Itk-G to I are composed of brownish silts. The sediments of Itk-I are exposed in a baidzharakh, because the two ice wedges around were extensively degraded (Fig. 1.20).
At Itk-G-02 and I-01 several black spots <5 mm are visible. The cryostructures change from latent micro-lenticular (Itk-G, Fig. 1.14f) to micro-porphyritic (Itk-H and I, Fig. 1.14g)

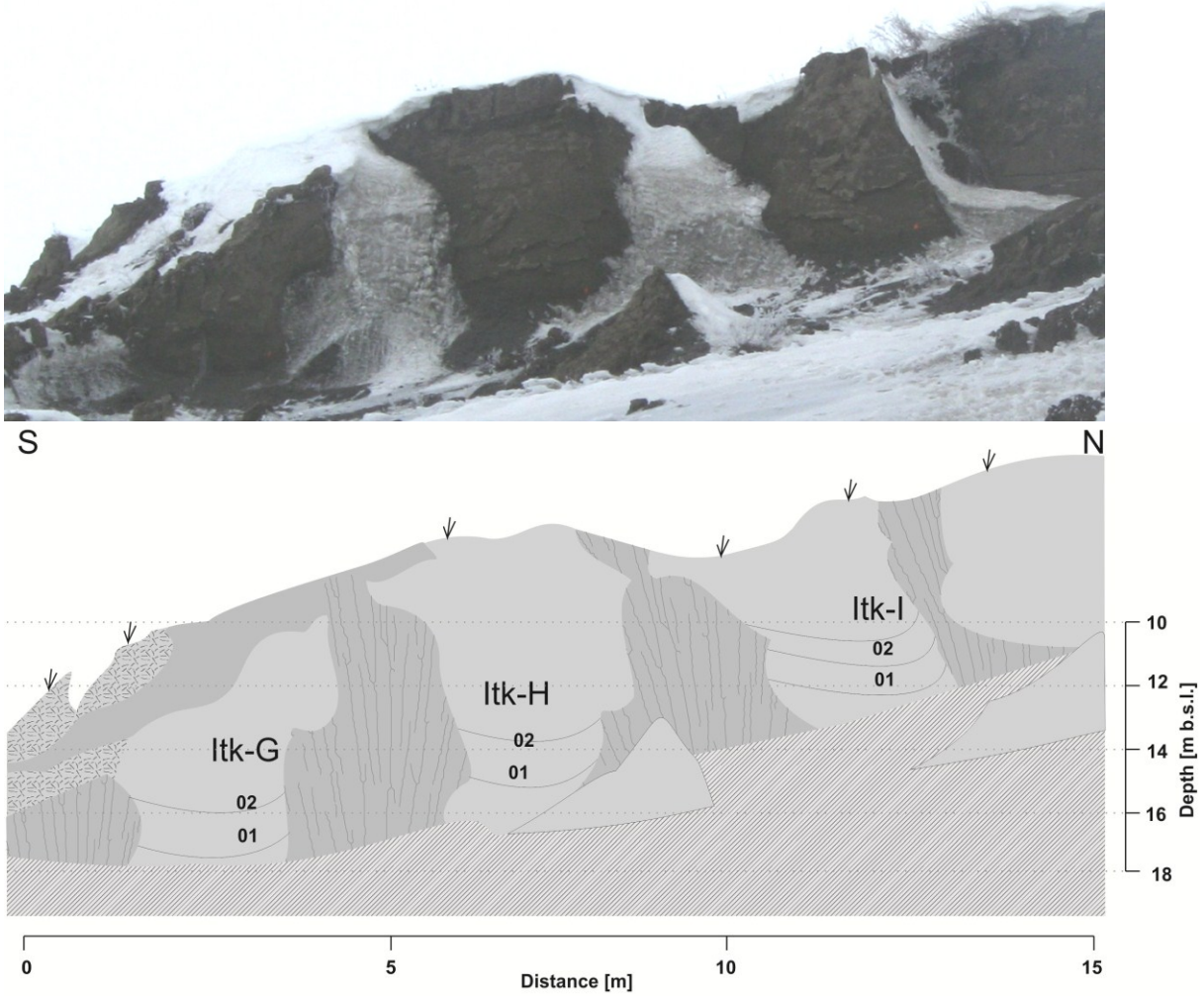

Fig. 1.20: *Picture and schematic of sub-profiles Itk-G, Itk-H and Itk-I. Picture a by K. Bjella (May 2012).*

Sub-profile Itk-E

The sub-profile ca. 70 m left of the major profile was exposed in a steep wall close to the top of the outcrop (Fig. 1.21). There, it was possible to climb a debris covered slope and to sample the bluff between 10.5 to 7.7 m b.s.l. using a ladder.
The samples Itk-E-01 to 03 are brownish and silty. The upper samples Itk-E-04 and -05 are more brownish than below with several black dots <5 mm. At the whole sub-profile Itk-E rootlets are present, but there are more rootlets in the upper two samples. The cryostructure is structureless (Fig. 1.14h) to latent micro-lenticular.
At this sub-profile, there are two large syngenetic ice wedges of ca 2 m width. Moreover, there are smaller ice wedges in the sediment column. At the very top of the sub-profile a Holocene white epigenetic ice wedge was observed.

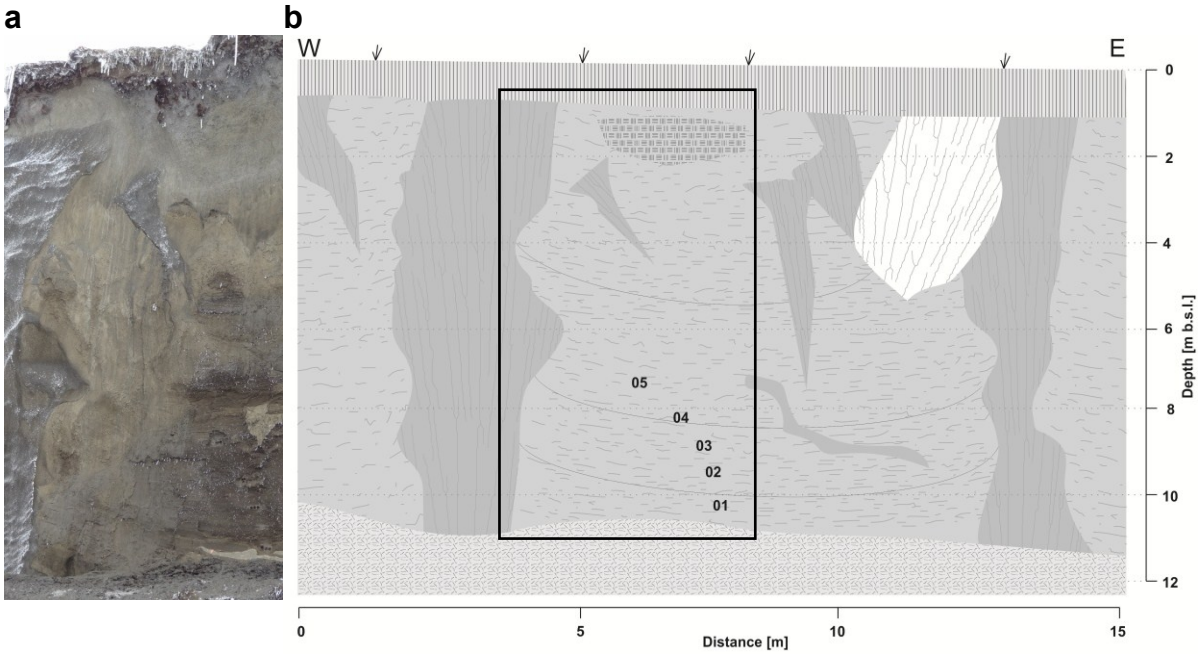

Fig. 1.21: *a) Picture and b) schematic of sub-profile Itk-E; the box in b marks the extent of the photograph in a. The sampled baidzharakh Fig. 1.19 is below this profile. Picture a by J. Strauss (May 2012).*

1.3. Drilling at Itkillik River Exposure

To study the modern ice-wedge degradation and thermokarst, two boreholes were cored on top of the exposure on the Yedoma hill. The boreholes were drilled using a SIPRE corer (7.5 cm and 5 cm in diameter). This core-drill was developed by the United States Snow, Ice and Permafrost Research Establishment (SIPRE). It takes a 7.5 cm or 5 cm core and can be used to core several meters by hand. It is driven with a motorized power head and raised and lowered by hand.

Fig. 1.22: *Drilling with an SIPRE-Corer at the top of the Yedoma hill. Picture by K. Bjella (May 2012)*

A GPS was used to survey the positions of the boreholes. The cores were drilled through completely frozen pond ice. The ponds are 20 to 30 cm deep, which formed above degrading ice wedges. The seasonally frozen soils at the bottoms of these ponds were 100 and 88 cm thick. That means, degradation of ice wedges in these

ponds is rather slow. This is caused by protection of the ice wedges by thick soil layers. At the selected coring sites, the soils are significantly thicker than the average active layer of the study area. Here, the seasonal thawing can reach ice wedges only at the end of summer.

Acknowledgements

We thank the National Science Foundation (NSF) for the financial support of the field trip within the frame of the cooperation project ARC-1023623. Jens Strauss acknowledges the German Federal Ministry of Education and Research for financial support (01DM12011). We would like to thank CH2M HILL Polar Services and pilot Dirk Nickisch for their logistical support.

References

Brown, J., O. J. Ferrians, J. A. Heginbottom, and E. S. Melnikov (1997), Circum-Arctic map of permafrost and ground-ice conditions, U.S. Geological Survey, Washington, D. C.

Carter, L.D., (1988) Loess and deep thermokarst basins in Arctic Alaska. Proceedings of the Fifth International Conference on Permafrost. Vol. 1 Tapir publishers, Trondheim, Norway, pp. 706–711.

Ehlers, J., and P. L. Gibbard (2003), Extent and chronology of glaciations, Quaternary Science Reviews, 22(15–17), 1561–1568, doi:10.1016/S0277-3791(03) 00130-6.

French, H., Shur, Y., 2010. The principles of cryostratigraphy. Earth-Science Reviews 110, 190–206. doi:10.1016/j.earscirev.2010.04.002.

Kanevskiy, M., Y. Shur, D. Fortier, M. T. Jorgenson, and E. Stephani (2011), Cryostratigraphy of late Pleistocene syngenetic permafrost (Yedoma) in northern Alaska, Itkillik River exposure, Quaternary Research, 75(3), 584–596, doi:10.1016/j.yqres.2010.12.003.

Péwé, T. L. (1975), Quaternary geology of Alaska, U.S. Geological Survey Professional Papers, 835, 145 pp.

Romanovskii, N. N. (1993), Fundamentals of Cryogenesis of Lithosphere, Moscow Univ. Press, Moscow, 336 pp.

Schirrmeister, L. , D. Froese, V. Tumskoy, G. Grosse, and S. Wetterich (in press), Yedoma: Late Pleistocene Ice-Rich Syngenetic Permafrost of Beringia, in Encyclopedia of Quaternary Science, 2nd Edition, edited by S. Elias, Elsevier, Amsterdam

Schirrmeister, L., G. Grosse, S. Wetterich, P. P. Overduin, J. Strauss, E. A. G. Schuur, and H.-W. Hubberten (2011), Fossil organic matter characteristics in permafrost deposits of the northeast Siberian Arctic, J. Geophys. Res., 116, G00M02, doi: 10.1029/2011jg001647.

Shur, Y. (1988), The upper horizon of permafrost soils, in Senneset, K. (ed), Proceedings of the Fifth International Conference on Permafrost, Tapir Publishers, Trondheim, Norway, pp. 867–871, Vol. 1

Strauss, J., L. Schirrmeister, S. Wetterich, A. Borchers, and S. P. Davydov (2012), Grain-size properties and organic-carbon stock of Yedoma Ice Complex permafrost from the Kolyma lowland, northeastern Siberia, Global Biogeochmeical Cycles, 26(GB3003), doi:10.1029/2011GB004104.

Wolfe, S. A., A. Gillis, and L. Robertson (2009), Late Quaternary Aeolian Deposits of Northern North America: Age and Extent, Geological Survey Of Canada, Ottawa, Ont., Canada, doi:10.4095/226434.

Appendix

A.1 Data from Previous Studies

According to previous studies of the Itkillik River exposure [Kanevskiy et al. 2011], this permafrost sequence comprised seven cryostratigraphical units (Fig. 1.23), including:

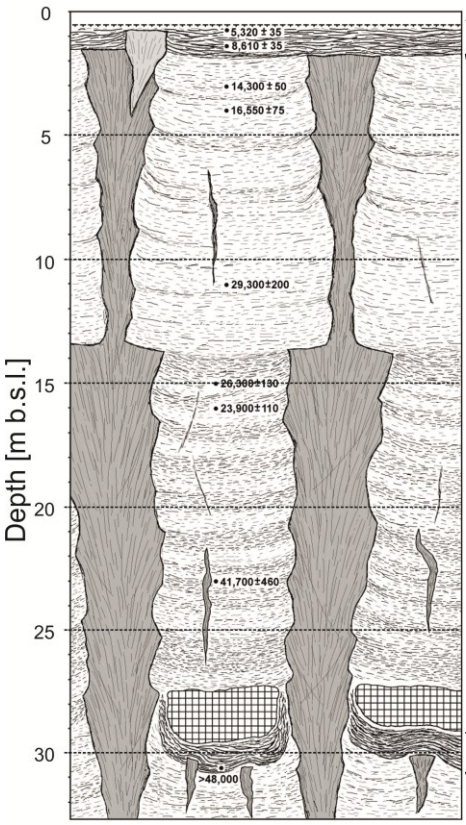

0 - 0.6 m	Unit 1 – Active layer (organic-rich brown-gray silt with fine sand).
0.6 - 1.5 m	Unit 2 – Contemporary intermediate layer (organic-rich yellow-gray silt; ice-rich; radiocarbon age from 5300 to 8600 ^{14}C a BP) with modern ice wedges.
1.5 - 13 m	Unit 3 – Yedoma with relatively thin ice wedges (yellow-gray and gray silt with rare small inclusions of organic matter; radiocarbon age from 14300 to 29300 ^{14}C a BP).
13 - 27 m	Unit 4 – Yedoma with thick ice wedges (yellow-gray and gray silt with rare small inclusions of organic matter; radiocarbon age from 23900 to 41700 ^{14}C a BP).
27 - 29 m	Unit 5 – Buried peat layer (dark-brown peat grading with depth into ice-rich organic silt).
29 - 30 m	Unit 6 – Buried intermediate layer (organic silt, ice-rich; radiocarbon age >48,000 ^{14}C a BP).
30 m to bottom	Unit 7 – Silt with small buried ice wedges.

Fig. 1.23: *Cryostratigraphical units of the Itkillik Yedoma (ice wedges width not to scale) and radiocarbon age of deposits, ^{14}C a BP, modified from Kanevskiy et al. [2011].*

The deposits of units 3 and 4 were formed from >48000 to 14300 ^{14}C years BP (Fig. 1.23 and Fig. 1.24), based on 11 radiocarbon dates from Kanevskiy et al. [2011] and six dates (three radiocarbon and three thermoluminescence dates) from Carter [1988]. The two youngest ages of Holocene age 5320 and 8610 ^{14}C a BP date the development of the intermediate layer [e.g. Shur, 1988]. At 15 m b.s.l., there was a wide range of dates. That corresponds to the transition from unit 3 to unit 4 (Fig. 1.24).

Grain-size distribution in eight samples [Kanevskiy et al. 2011] revealed a homogeneous composition of the deposits, which are composed mainly of silt (up to 83 wt%). The average organic carbon content of the Yedoma deposits is 0.4 wt%. Compared to other Yedoma sequences [e.g. Schirrmeister et al. 2011], this is very low. The Itkillik Yedoma has a very high content of wedge ice (Fig. 1.25). There are four generations of wedge-ice, which are attributed to distinct periods of formation. Relatively thin and short Holocene ice wedges occur within the intermediate layer

(Unit 2). These wedges are up to 1 to 2 m wide and up to 3 to 4 m tall, wedge shaped-and actively forming. Ice wedges in Unit 3 are relatively wide at the top (up to 3 to 4 m) and their width decreases gradually with depth.

In lower part of the unit (at depths from 6 to 7 m to 13 to 14 m), the width of ice wedges rarely exceeds 1 to 2 m. The spacing between ice wedges varies from 7 to 10 m. Ice wedges in Unit 4 are up to 5 to 7 m wide and their width remains nearly constant with depth. Their total vertical size cannot be determined because most of it continues below the Itkillik River water level. Ice wedges in Unit 7, located at the bottom of the exposure beneath the peat layer, are less than 0.7 m in width and 2.5 to 3 m in height. The spacing between ice wedges varies from 3 to 8 m. In order to estimate the wedge-ice volume, Kanevskiy et al. [2011] combined numerous composite black & white images of ice wedges (Fig. 1.25). Based on measurements of the areas occupied by wedge ice in these images, wedge-ice volume varies from 40 to 52% in cryostratigraphic units 2 to 3, and is 78% in units 4 to 7 (calculations were performed for the 240 m central section of the exposure). On average, wedge ice occupies 57% of the entire exposed bluff (Fig. 1.26).

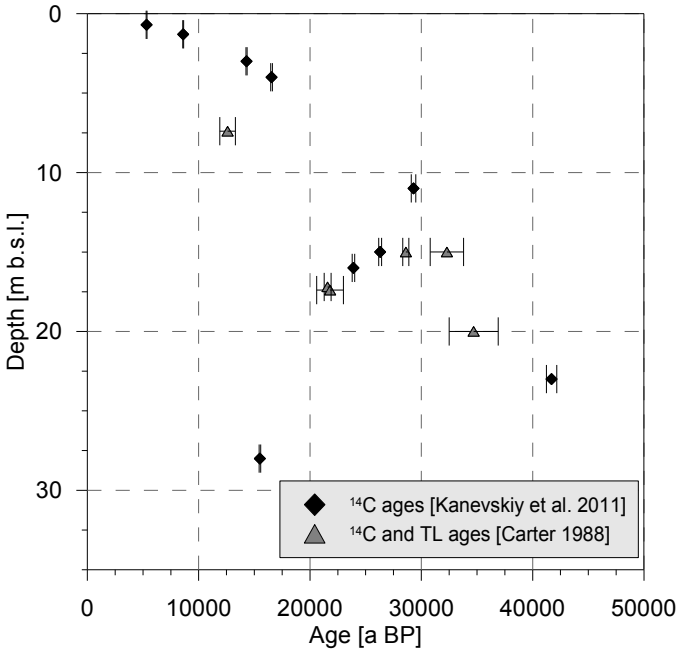

Fig. 1.24: *Age-depth relationship of the Itkillik Yedoma, based on radiocarbon and thermoluminescence analyses*

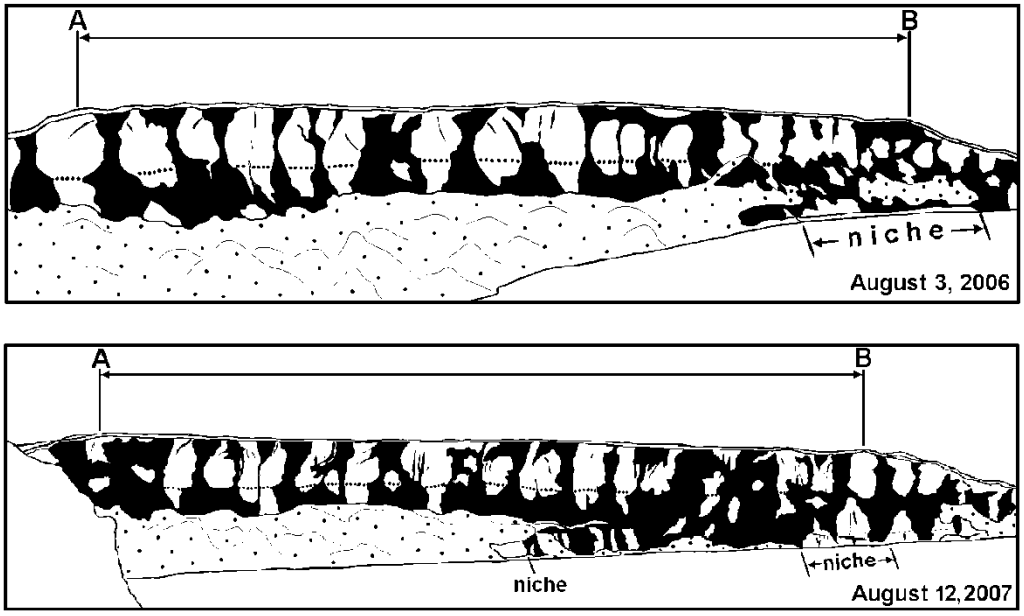

Fig. 1.25: *Appearance of wedge-ice (black) in the Itkillik River exposure on August 3, 2006 and August 12, 2007. AB – central part of the bluff with flat Yedoma surface, the length is 240 m. Dotted line shows the boundary between Units 3 and 4 (modified from Kanevskiy et al. [2011]).*

In contrast to the ice wedge content, the intrasedimentary ice (segregaded and pore ice) content is low. The total volume of ground ice including wedge ice, intrasedimentary and segregated ice between ice wedges is 90% in Unit 4 and 83% for the entire bluff (Fig. 1.26).

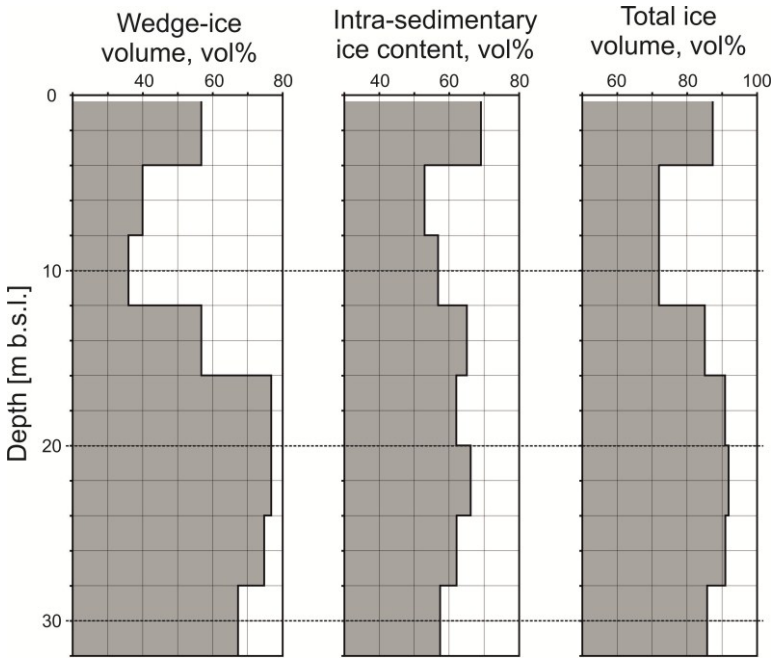

Fig. 1.26: *Percent volume of wedge, segregated, and intrasedimentary ice with depth in the Itkillik River exposure. Modified from Kanevskiy et al. [2011].*

A.2 Participating institutions - Alaskan North Slope / Itkillik 2012

	Address
AWI	Alfred-Wegener-Institute for Polar- and Marine Research, Periglacial Research Unit Telegrafenberg A43 14473 Potsdam Germany
CRREL	United States Army Corps of Engineers, Cold Regions Research and Engineering Laboratory, Engineering Research and Development Center P.O. Box 35170 Fort Wainwright, Alaska 99703 United States of America
UAF	University of Alaska Fairbanks, Institute of Northern Engineering PO Box 755910 539 Duckering Building 306 Tanana Loop University of Alaska Fairbanks Fairbanks, Alaska 99775-5910 United States of America
UdeM	Université de Montréal Département de géographie Geocryolab 520, chemin Côte-Ste-Catherine Montréal, Québec, H2V 2B8 Canada

A.3 Expedition Participants - Alaskan North Slope / Itkillik 2012

Last name	First name	Institute	Profession
Bjella	Kevin	U.S. Army Cold Regions Research and Engineering Laboratory (CRREL)	Research civil engineer
Breen	Amy	University of Alaska Fairbanks (UAF)	Biologist, Postdoctoral Fellow
Fortier	Daniel	Université de Montréal (UdeM)	Geomorphologist, Assistant Professor
Johnson	Cody	CH2M HILL Polar Services	Science project manager, Biologist
Kanevskiy	Mikhail	University of Alaska Fairbanks (UAF)	Geologist, Research Assistant Professor
Shur	Yuri	University of Alaska Fairbanks (UAF)	Geologist, Professor
Strauss	Jens	Alfred-Wegener-Institute	Geoecologist, PhD student,

A.4 Sample Lists - Alaskan North Slope / Itkillik 2012

Tab. A.4.1.3: *List of sediment samples*

sample	depth [m]	sediment description	cryostructure	visible organic matter	remarks	coordinates (N)	coordinates (W)	sampling date	sampled by
1	22.3					69°34'03.5"	150°51'57.2"	11/05/2012	Cody Johnson
2	20.8		micro-(braided) lenticular		peat layer right below sampling point	69°34'03.5"	150°51'57.2"	11/05/2012	Cody Johnson
14C-1	20.6				peat layer sampled for radiocarbon dating	69°33'56.7"	150°51'33.7"	14/05/2012	Jens Strauss
It-1	2.3		micro-braided to micro-ataxitic			69°34'03.5"	150°51'57.2"	12/05/2012	Cody Johnson
It-2	4.7					69°34'03.5"	150°51'57.2"	12/05/2012	Cody Johnson
It-3	7.2		porphyritic			69°34'03.5"	150°51'57.2"	12/05/2012	Cody Johnson
It-4	8.9		porphyritic			69°34'03.5"	150°51'57.2"	12/05/2012	Cody Johnson
It-5	0.5					69°34'03.5"	150°51'57.2"	13/05/2012	Cody Johnson
It-6	5.4		structureless			69°34'03.5"	150°51'57.2"	13/05/2012	Cody Johnson
It-7	20.5					69°34'03.5"	150°51'57.2"	13/05/2012	Cody Johnson
It-8	9.7		micro-lenticular			69°34'03.5"	150°51'57.2"	13/05/2012	Cody Johnson
It-9	21.3		micro-(layered) lenticular			69°34'03.5"	150°51'57.2"	13/05/2012	Cody Johnson
Itk-B-01	28.0	silty, brownish	(micro-) lenticular	marcro (rarely)	rests	69°34'03.2"	150°51'56.0"	11/05/2012	Jens Strauss
Itk-B-02	27.5	silty, brownish	micro-lenticular to micro-braided	marcro (rarely)	rests	69°34'03.2"	150°51'56.0"	11/05/2012	Jens Strauss
Itk-B-03	27.0	silty, brownish	(micro-) lenticular	marcro (rarely), rootlets	rests	69°34'03.2"	150°51'56.0"	11/05/2012	Jens Strauss
Itk-B-04	26.5	silty, brownish	(micro-) lenticular	few inclusions, organic plant remains		69°34'03.2"	150°51'56.0"	11/05/2012	Jens Strauss
Itk-C-01	26.4		lenticular	macro (rarely)	rests	69°34'03.5"	150°51'57.2"	12/05/2012	Jens Strauss
Itk-C-02	25.9		lenticular	marco remains		69°34'03.5"	150°51'57.2"	12/05/2012	Jens Strauss

sample	depth [m]	sediment description	cryostructure	visible organic matter	remarks	coordinates (N)	coordinates (W)	sampling date	sampled by
Itk-C-03	25.5		porphyritic	marco remains		69°34'03.5"	150°51'57.2"	12/05/2012	Jens Strauss
Itk-C-04	25.1		lenticular, thick ice band 5cm above sampling point. Same ice band like at Itk-D-1	macro rests (rarely)		69°34'03.5"	150°51'57.2"	12/05/2012	Jens Strauss
Itk-D-01	25.7	silty, brownish	micro-(braided) lenticular	plant remains (rarely)	bigger ice band <3cm 10cm below sampling point	69°34'03.5"	150°51'57.2"	12/05/2012	Jens Strauss
Itk-D-02	25.0	silty, brownish	braided to ataxitic (suspended)	not visible		69°34'03.5"	150°51'57.2"	12/05/2012	Jens Strauss
Itk-D-03	24.8	silty, brownish	ataxitic			69°34'03.5"	150°51'57.2"	12/05/2012	Jens Strauss
Itk-D-04	24.3		braided lenticular, ice bands up to 2cm thick,			69°34'03.5"	150°51'57.2"	13/05/2012	Jens Strauss
Itk-D-05	24.0	darker sediment	braided lenticular, ice bands >2cm thick	peat inclusions		69°34'03.5"	150°51'57.2"	13/05/2012	Jens Strauss
Itk-D-06	23.8		lenticular	macro rests (rarely)		69°34'03.5"	150°51'57.2"	13/05/2012	Jens Strauss
Itk-D-07	23.3		ataxitic			69°34'03.5"	150°51'57.2"	13/05/2012	Jens Strauss
Itk-D-08	22.5	peat layer			sample for radiocarbon dating from peat layer	69°34'03.5"	150°51'57.2"	13/05/2012	Jens Strauss
Itk-E-01	10.5		(latent) micro lenticular	rootlets		69°34'05.9"	150°52'06.8"	13/05/2012	Mikhail Kanevskiy
Itk-E-02	9.8		micro-lenticular	rootlets		69°34'05.9"	150°52'06.8"	13/05/2012	Mikhail Kanevskiy
Itk-E-03	9.2		latent micro-lenticular	rootlets		69°34'05.9"	150°52'06.8"	13/05/2012	Mikhail Kanevskiy

sample	depth [m]	sediment description	cryostructure	visible organic matter	remarks	coordinates (N)	coordinates (W)	sampling date	sampled by
ltk-E-04	8.4	more brownish than below, several black dots <5mm	micro-lenticular	many rootlets		69°34'05.9"	150°52'06.8"	13/05/2012	Mikhail Kanevskiy
ltk-E-05	7.8	more brownish than below, several black dots <5mm	(latent) micro lenticular	many rootlets	not drilled, taken with hammer and chisel	69°34'05.9"	150°52'06.8"	13/05/2012	Jens Strauss
ltk-F-01	21.0	several black dots 1-2 mm	micro-(braided) lenticular			69°34'05.3"	150°52'07.3"	13/05/2012	Jens Strauss
ltk-F-02	20.2		micro-lenticular to lenticular, ice filled crack 10cm below	rootlets, macro rests (rarely)		69°34'05.3"	150°52'07.3"	13/05/2012	Jens Strauss
ltk-F-03	19.5	several black dots 1-2 mm	porphyritic, 2 ice bands, 1-2mm thick	rootlets		69°34'05.3"	150°52'07.3"	13/05/2012	Jens Strauss
ltk-G-01	16.8		micro-lenticular	rootlets		69°34'05.6"	150°52'13.0"	14/05/2012	Mikhail Kanevskiy
ltk-G-02	15.9	several black dots <5 mm	micro-lenticular to micro-braided	rootlets		69°34'05.6"	150°52'13.0"	14/05/2012	Mikhail Kanevskiy
ltk-H-01	14.7			rootlets (rarely)		69°34'05.4"	150°52'12.4"	14/05/2012	Mikhail Kanevskiy
ltk-H-02	13.7		micro-lenticular	rootlets		69°34'05.4"	150°52'12.4"	14/05/2012	Mikhail Kanevskiy
ltk-I-01	11.9	black spots	micro-porphyritic	rootlets		69°34'06.2"	150°52'13.0"	14/05/2012	Mikhail Kanevskiy
ltk-I-02	10.6		micro-porhyritic			69°34'06.2"	150°52'13.0"	14/05/2012	Mikhail Kanevskiy
ltk-J-01	29.8		(latent) micro lenticular	macro rests (very rare)		69°34'04.6"	150°52'05.1"	14/05/2012	Mikhail Kanevskiy
ltk-J-02	28.9		structureless			69°34'04.6"	150°52'05.1"	14/05/2012	Mikhail Kanevskiy
ltk-J-03	28.3		micro-lenticular			69°34'04.6"	150°52'05.1"	14/05/2012	Mikhail Kanevskiy

Tab. A.4.1.4: *List of horizontal ice-wedge samples*

sample	depth [m]	horizontal position [cm]	sampled by
IR-1/12	26.8	0	Mikhail Kanevskiy
IR-2/12	26.8	25	Mikhail Kanevskiy
IR-3/12	26.8	50	Mikhail Kanevskiy
IR-4/12	26.8	75	Mikhail Kanevskiy
IR-5/12	26.8	100	Mikhail Kanevskiy
IR-6/12	26.8	125	Mikhail Kanevskiy
IR-7/12	26.8	150	Mikhail Kanevskiy
IR-8/12	26.8	175	Mikhail Kanevskiy
IR-9/12	26.8	200	Mikhail Kanevskiy
IR-10/12	26.8	225	Mikhail Kanevskiy
IR-11/12	26.8	250	Mikhail Kanevskiy
IR-12/12	26.8	275	Mikhail Kanevskiy
IR-13/12	26.8	300	Mikhail Kanevskiy
IR-14/12	26.8	325	Mikhail Kanevskiy
IR-15/12	26.8	350	Mikhail Kanevskiy
IR-16/12	26.8	375	Mikhail Kanevskiy
IR-17/12	26.8	400	Mikhail Kanevskiy
IR-18/12	26.8	425	Mikhail Kanevskiy
IR-19/12	26.8	450	Mikhail Kanevskiy
IR-20/12	26.8	475	Mikhail Kanevskiy
IR-21/12	26.8	500	Mikhail Kanevskiy
IR-22/12	26.8	525	Mikhail Kanevskiy
IR-23/12	26.8	560	Mikhail Kanevskiy

Tab. A.4.1.5: *List of vertical ice-wedge samples*

sample	depth [m]	sampled by
IR-24/12	2.3	Amy Breen
IR-25/12	4.5	Amy Breen
IR-26/12	7.1	Amy Breen
IR-27/12	9.2	Amy Breen

sample	depth [m]	sampled by
IR-28/12	11.5	Amy Breen
IR-29/12	13.7	Amy Breen
IR-30/12	15.6	Amy Breen
IR-31/12	17.7	Amy Breen
IR-32/12	19.4	Amy Breen
IR-33/12	21.5	Amy Breen
IR-34/12	23.6	Amy Breen
IR-35/12	24.6	Amy Breen
IR-36/12	25.6	Amy Breen
IR-37/12	27.6	Amy Breen

2. THERMOKARST IN CENTRAL YAKUTIA 2012

Project Initiation Field Trip for a Study of Short and Long-term Thermokarst Dynamics due to Climate Changes and Human Impacts in Central Yakutia, Siberia

Mathias Ulrich, Christine Siegert, Alexander N. Fedorov

2.1. Expedition Background

Current periglacial research has a focus on thermokarst processes in ice-rich permafrost deposits in Siberia [e.g. Morgenstern et al., 2011] and the North American Arctic [e.g. Jones et al., 2012]. Thermokarst basins of several square kilometers (*alases*, up to ~50 km²), often filled with lakes and separated by flattened hills (*Yedoma* uplands) of ice-rich deposits (Ice Complex), are the most striking landscape elements in Eastern Siberia. Approximately 30% from the East Siberian area is occupied by ice-rich deposits [Sazonova et al., 2004]. Parallel to the pronounced climate changes in arctic permafrost regions [e.g. Romanovsky et al., 2010], essential changes in permafrost conditions (i.e. increasing ground temperatures and active layer depth) were observed in the subarctic and boreal zones of Central Yakutia [e.g. Sazonova et al., 2004; Fedorov & Konstantinov, 2009]. These changes in permafrost conditions within the populous region of Central Yakutia have already been resulted and will result in impacts on infrastructure and land use due to changes in frozen ground stability and surface hydrology. The thawing of permafrost might also result in significant impacts on the global carbon cycle, because warming can possibly cause a release of old carbon pools from ice-rich deposits [e.g. Walter et al., 2006; Grosse et al., 2011]. However, driving factors of thermokarst are not well understood yet due to complex geological, geomorphological, hydrological, ecological, climatic, and geocryological interrelations.

A 14 day field trip was undertaken in July 2012 in the thermokarst landscapes around Yakutsk, Russia. The focus of the expedition has been on the reconnaissance of thermokarst key areas in the region. Besides, the exchange of experience and the evaluation of archive data has been a second focus. First orienting investigations were made as basis for a planned research project about the Holocene and modern thermokarst dynamics in Central Yakutia and their natural and anthropogenic influencing factors as well as the evaluation of future landscape evolution (DFG UL426/1-1, Short and long-term thermokarst dynamics due to climate changes and human impacts in Central Yakutia, Siberia, submitted 06/2012). Detailed field knowledge was necessary to both, the scientific and logistical point of view, to select suitable study sites from the plurality of permafrost degradation landforms. Secondly, this information serves as a basis for the initial validation of satellite data. Additionally, a further emphasis was the clarification of necessary logistic support from Russian side during the planned project.

Main Emphases of the Journey

- Experience exchange and presentation of former studies. Survey and examination of lab, staff, and equipment (i.e. drill equipment, etc.) capacity at the Melnikov Permafrost Institute in Yakutsk
- Archive data inquiry at Melnikov Permafrost Institute in Yakutsk
- Logistical arrangements (i.e. transportation and accommodation during future field campaigns, existing and required hardware, handling and transportation of soil samples, custom procedures, rules for research permit)
- Selection of key sites for thermokarst studies by surveying of the specific geomorphological situations on different Pleistocene terraces right and left of the Lena River
- First time analysis of periglacial surface characteristics, in particular of different thermokarst depression units and inter-alas areas (Ice Complex)
- First time selection and study of diverse permafrost sediment sequences with regard to thermokarst processes (i.e. preliminary assessment of cryolithological, sedimentological, and stratigraphic properties)
- Preliminary sampling for initial sedimentological, geochemical, and geochronological analyses
- Preliminary botanical survey of different thermokarst depression units and inter-alas areas as ground truth for remote sensing studies

2.2. Itinerary and Journey Participants

For the exploration trip, two scientists of the Alfred Wegener Institute for Polar and Marine Research (AWI Potsdam; Christine Siegert, Mathias Ulrich) went immediately after the Tenth International Conference on Permafrost (TICOP) held in Salekhard, Russia, to Yakutsk to meet with permafrost scientists of the Melnikov Permafrost Institute (PIY). After a 3-day stay in Yakutsk at the PIY, a joined 8-day field trip was undertaken together with scientists of the Yakutsk State University (YSU) and of the Institute for Biological Problems of the Cryolithozone (IBPC) (Fig. 2.1). A four-wheel-drive car was used to go to the right side of the Lena River; the Lena-Aldan-Amga interfluves region. During the journey, two field camps were used as base for exploring different kinds of thermokarst landscape features. The trip itinerary is shown in Tab. 2.1.

Fig. 2.1: Participants of the project initiation trip (f.l.t.r.): Shanna Degteva (YSU), Yuri G. Danilov (YSU), Alexander N. Fedorov (PIY), Mathias Ulrich (AWI), Christine, Siegert (AWI), Roman V. Desyatkin (IBPC), Junior scientist at IPBC

Tab. 2.1: *Time table for the journey*

Date	Location	Task
01.-04.07.2012	Melnikov Permafrost Institute in Yakutsk	Preparations, consultations, discussions, presentation, and data acquisition
05.07.2012	Yakutsk and Yukechi study site	Departure from Yakutsk to the right-side of the Lena River with car and crossing the river by ferry
05.-08.07.2012	Yukechi study site	Exploration trips and field work in and around the Yukechi study site and on the Abalakh terrace
08.-10.07.2012	Ulakhan Sekhan study site	Exploration trips and field work in and around the Ulakhan Sekhan study site and on the Tyungyulyu terrace
10.07.2012	Ulakhan Sekhan study site and Yakutsk	Departure from Ulakhan Sekhan to Yakutsk with car and crossing the river by ferry
11.07.2012	Neleger study site	Exploration trip to the Neleger study site on the high terrace on left-side of the Lena River
11.-14.07.2012	Melnikov Permafrost Institute in Yakutsk	Final consultations, discussions, and data acquisition

2.3. Study Region and General Geomorphological Description

Central Yakutia is characterized by a strong continental climate with low annual precipitation (250-300 mm), a mean annual air temperature of -8.7°C, and a high seasonal temperature gradient during the year of 80 to 100°C with minimum January temperatures of about -60°C (mean -43°C to -38°C) and maximum July temperatures of about 40°C (mean 16-19°C; Meteorological station Yakutsk; www.meteo.ru). Distinct lowering of water levels of thermokarst lakes occurs during summer due to high evaporation rates (annual mean 350-400 mm). Permafrost has been reported to reach depths of between 400 and 700 m. The active layer (i.e. the upper layer of the ground which thaws seasonally) reaches only depths of 0.5 -2.0 m [Matveev, 1989].
The study region in Central Yakutia is bounded by the Lena, Aldan, and Amga rivers (Fig. 2.2). Major parts of this interfluves region consist of ice-rich deposits (i.e. Ice Complex, Yedoma). Several terraces above the major rivers are differentiated due to sediment lithology and genesis. Four terraces are geomorphologically classified with regard to Ice Complex accumulation and degradation [Soloviev, 1973].

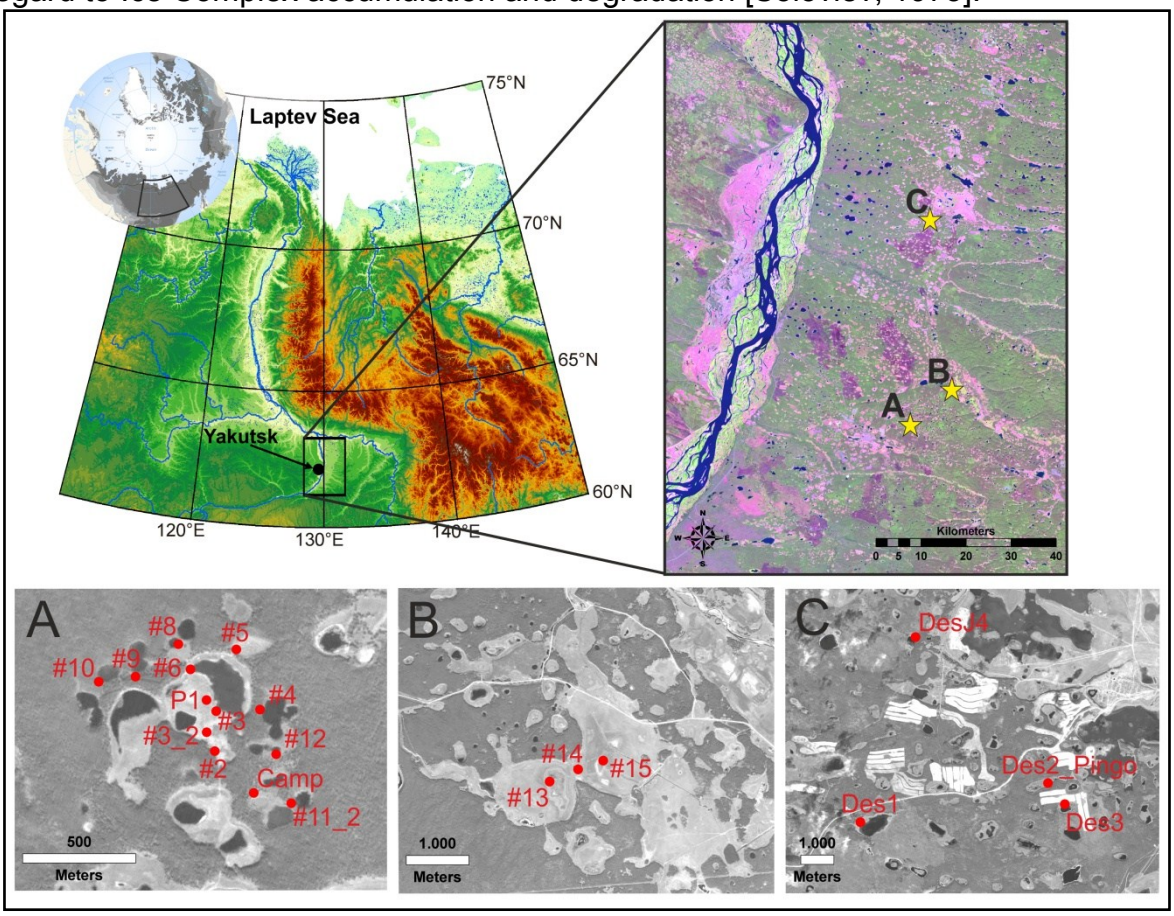

Fig. 2.2: *Study region in Eastern Siberia within the zone of continuous permafrost and thermokarst key sites in the Lena-Aldan-Amga region explored during the journey. The labeled red points indicate GPS-located sites of detailed surface description and preliminary sedimentological surveys. A: Yukechi study site on the Abalakh terrace. B: Khara Bulgunakh alas on the Tyungyulyu terrace. C: Investigated sites around the Ulakhan Sekhan study site on the Tyungyulyu terrace. Upper left: Digital elevation model of East Siberia compiled by data of the ESA DUE Permafrost project; http://www.ipf.tuwien.ac.at/permafrost/. Upper right: Close up of a Landsat-TM5 image, August 12, 2002; RGB 5-4-3. Below: AlosPrism close ups, August 13, 2010.*

Typical well-developed alas basins are found mainly on the *Tyungyulyu* and *Abalakh* terraces, 65 to100 m and 115 to 135 m a.r.l., respectively. Both terraces are characterized by thick ice-rich deposits (>25 m in some places) but they show different characters of thermokarst landforms. While large thermokarst basins (e.g. *Tyungyulyu* and *Myuryu alases*) and thermokarst landforms in different generations are dominating the *Tyungyulyu* terrace, the higher *Abalakh* terrace is characterized by a more dissected thermokarst relief and a higher density of *alases* as well as by recent thermokarst activity [Fedorov & Konstantinov, 2003; 2009].

2.4. Preliminary Results and Initial Findings

The major aim of the journey was the exploration and the characterization of different relief units and geomorphological features in the context of permafrost degradation processes and permafrost landscape evolution. Different field sites were explored, which provides exemplary first time information on the local scale as well as ground truth data for preliminary remote sensing analyses. The parameters described and explored comprise relief features, vegetation properties, and hydrological characteristics. The depth of the active layer was determined exemplarily by ramming a steel pole into the ground until the permafrost table was reached. One soil-sediment profile and 3 lakes at the *Yukechi* study site (Fig. 2.2A) were exemplary sampled for orienting lab analyses. The different field sites on the different geomorphological terraces are clearly distinguishable with regard to form, degree, and activity of thermokarst processes. Here, variations in the lithology of the underlying sediments and of the Ice Complex likely play a crucial role.

Yukechi Study Site

The *Yukechi* study site, located on the *Abalakh* terrace (Fig. 2.2A), is characterized by many young thermokarst features surrounding a larger alas system. Different stages of thermokarst development proposed by e.g. Soloviev [1973] are well recognizable in the area. Several small young thermokarst lakes could be explored. Many of these lakes were evidently developed anthropogenically (e.g. in former agricultural areas) or naturally (e.g. after forest fires) within the last 40 years (Fig. 2.3). These lakes, currently remaining in the *Tympa* stage [Soloviev, 1973], are no larger than 100 m in diameter (see e.g. Point #8, #9, and #10 in Fig. 2.2A) and show very strong lake shore expansion in all directions (~1-2 m/year) destroying the surrounding taiga forest (Fig. 2.4). Some lakes are coalescing very quickly (see e.g. Point #4 in Fig. 2.2A) and one dried basin could be explored at the *Yukechi* site (see Point #5 in Fig. 2.2A), were the lake was drained trough a narrow valley into the larger *Yukechi* alas just 3 years ago (Fig. 2.5). Current thermokarst processes, mainly initiated by an increase in the active layer depth, could be explored at several areas, which remain in the initial *Bylar* stage [Soloviev, 1973]. The thawing of ice-wedges and thus the degradation of the underlying Ice Complex polygonal network led to characteristic hillocky surfaces where the former polygonal centers remain upstanding as thermokarst mounds (*Baidzharakhs*; Fig. 2.6). In these areas, the Russian colleagues could measure an increase in surface subsidence during the last decade (5-10 cm/yr; e.g. Fedorov and Konstantinov [2009]).

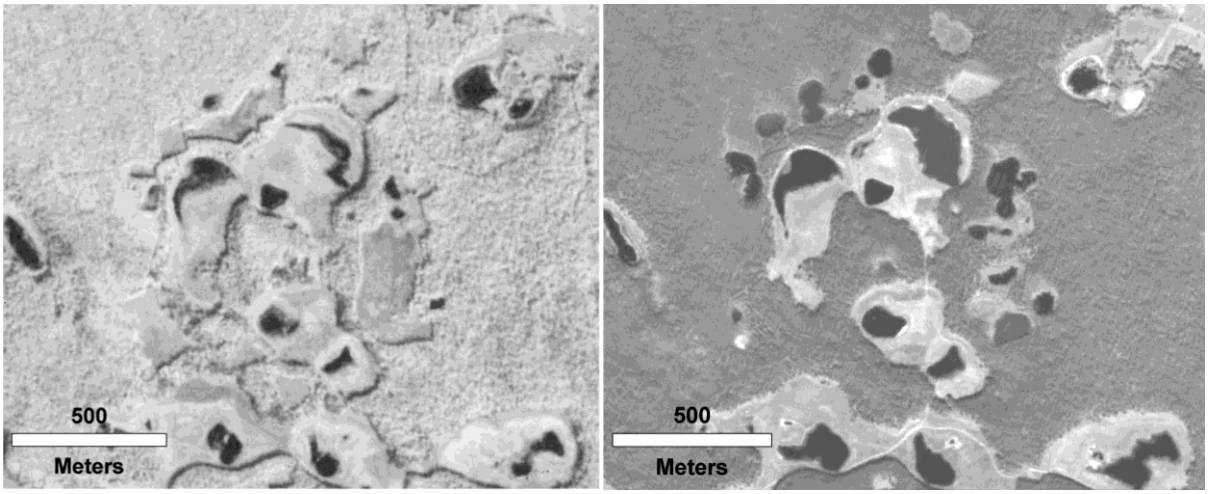

Fig. 2.3: *Landscape evolution at the Yukechi study site. Several thermokarst lakes in the north and the southeast of the Yukechi alas have been developed since 1967 (left), in particular in areas which were used agriculturally before (Compare e.g. Point #8, #9, and #10 in Fig. 2.2A). Left: Close up of a Corona image, September 20, 1967. Right: AlosPrism close up, August 13, 2010.*

Fig. 2.4: *Panoramic view of an expanding thermokarst lake in the Tympa stage at the Yukechi study site (Point 11_2 in Fig. 2.2A)*

Fig. 2.5: *Left: Basin of a recently drained thermokarst lake. Note the already dense vegetated Baidzharakhs (thermokarst mounds) at the basin bottom. Right: The drainage channel to the Yukechi alas cutting the Ice complex uplands.*

Fig. 2.6: *Left: Active ground-ice thawing and surface subsidence led to the development of Baidzharakhs close to the camp site (see Fig. 2.2A). Right: Small area of initial thermokarst. However, current surface subsidence could not be measured here by the Russian scientists. Probably, this is cause by the lack of water availability at this site.*

The *Yukechi* alas (Fig. 2.7) was explored as one of the expected thermokarst key sites in the proposed project in more detail. One soil-sediment profile (P1 in Fig. 2.2A, about 1.60 deep) and 3 lakes within the alas were exemplary sampled for orienting lab analyses. The *Yukechi* alas is about 500 m in diameter and about 7 m deep. Two larger and one small lake existed within the alas. During the time of the field trip all lakes were measured to be about 2-3 m deep. Although the steel pole was rammed into the ground until a depth of about 2.80 m, the depth of the permafrost table could not be measured. Probably, a talik (i.e. a body of unfrozen ground developing below large lakes) still exist below the basin, which could have been formed by a larger lake filling the alas previously. The general geomorphology of the alas (Fig. 2.2A) and different elevated ground levels of the alas bottom suggests that the current alas system was formed by the coalescence of 3-4 larger (lake-) basins. Higher ground levels are likely a sign for spatial differences in the lithology and ground-ice contents of the underlying Ice Complex. Lower ground-ice contents would have had reduced the surface subsidence below developing thermokarst lakes. The surface of the present-day alas bottom is very dry and dominated mainly by reddish halophytic grasses. The alas is bounded by steep slopes showing signs of erosion and slope movement. The forest covering the Ice Complex uplands around the alas normally ends at the upslope edges (Fig. 2.7).

Fig. 2.7: *Panoramic view from North (Point #6 in Fig. 2.2A) to South in the eastern part of the Yukechi alas system.*

Khara Bulgunakh

Khara Bulgunakh is part of a large alas system on the *Tyungyulyu* terrace about 20 km further northeast from the *Yukechi* study site. The system is formed by the *Khara Bulgunakh* alas which is about 1000 m in diameter and 5 m deep and the north to south stretching alas *Ulakhan Ebe* (Fig. 2.2B).
The alas system is a good example for the intensive agricultural use of large alases in the Lena-Aldan-Amga interfluves region east of Yakutsk (Fig. 2.8). Large parts of the alas bottom are used for cereal cultivation, hay farming, and pasturing. With regard to sometimes extreme annual and seasonal lake level changes in the region, the alas is drained trough an artificial drainage channel to avoid cropland flooding.

Fig. 2.8: *Anthropogenic use of the alas system Khara Bulgunakh – Ulakhan Ebe. Left: Extensive cereal cultivation. Due to the very dry climate, the fields have to be irrigated artificially. Right: Livestock grazing in the image background in front of the forested alas slope. The drainage channel can be seen in the centre of the picture.*

This alas system is characterized by the existence of three pingos (i.e. perennial ice-cored mounds formed by talik refreezing and water injection) (Fig. 2.9; Point #13, #14, and #15 in Fig. 2.2B). Pingos are particularly widespread on the *Tyungyuluy* terrace as sandy deposits below the Ice Complex providing the water-bearing layers necessary for pingo genesis. In contrast, less pingos can be found on the higher *Abalakh* terrace as it is build mainly by clayish-silty sediments.
The *Khara Bulgunakh* pingos line up like a string of pearls (Fig. 2.2B) probably marking the deepest contours of the coalesced alas basins. The degradation of the pingos (i.e. indication for thawing of inner ice core) is increasing from east (Point #15 in Fig. 2.2B) to west (Point #13 in Fig. 2.2B) and the heights are decreasing. The eastern pingo is the largest with about 10 m height and a horizontal dimension of about 100 m. This pingo is conical-shaped and only small cracks on the top are suggesting initial degradation. The tops of the middle and the western pingo are already collapsed. Both pingos are about 7-8 m high. The former centres are marked by depressions filled with vegetated ponds. However, the depression on the western pingo (Point #13) is flanked by two lines of circular ridges suggesting at least two different stages of ice-core collapse and growing. Interestingly, the active-layer depth was measured to be only about 1.00-1.20 m within the depressions of the two collapsed pingos. This suggests that the ice cores still exists immediately below the surface sediment layer. Finally, all three pingos are showing a ~1 m high zone of

fresh vegetation at their lower flanks (Fig. 2.9), obviously marking recently higher lake water levels in the alas system. During the time of the field trip, small and very shallow lakes are surrounding only the western and the middle pingo (Point #13 and #14, Fig. 2.2B).

Fig. 2.9: *The pingos in the Khara Bulgunakh – Ulakhan Ebe alas system. The degradation of the pingos is decreasing and the heights are increasing from left to right (from west to east in Fig. 2.2B).*

Around Ulakhan Sekhan

The exploration of the last sites during the field journey was guided by Prof. R.V. Desyatkin (Deputy Director of the Institute for Biological Problems of the Cryolithozone in Yakutsk). Some sites were visited together to get a closer view on thermokarst processes on the *Tyungyulyu* terrace (Fig. 2.2C). The sites are partly investigated by the Russian colleagues since decades. The long-term investigations within different alases include studies of soils and plant communities and their changes, the mapping of lake level change, and cryolithological studies [e.g. Desyatkin, 2008].

In general, the alases on the *Tyungyulyu* terrace are larger than on the *Abalakh* terrace. Alas slopes are often less steep and forested. One of the largest alas in the Lena-Aldan-Amga region is the *Tyungyulyu* alas with about 10 km in diameter (partly seen in the upper right corner of Fig. 2.2C). During the 1940s, the alas was filled completely by a large lake. Today, many small lakes are distributed within the basin. The huge grasslands within the alas are extensively used for farming and pasturing (Fig. 2.10).

Fig. 2.10: *Panoramic view on the Tyungyulyu alas from the southern alas slopes. The alas is one of the largest alas in the Lena-Aldan-Amga region with a dimension of about 10 km and a depth of about 10 m.*

A second camp site was used during the journey close to the *Ulakhan Sekhan* alas (Des1 in Fig. 2.2C). The research group of Prof. Desyatkin leases this alas for investigation of the natural development of thermokarst landscapes as it is not used

agriculturally before. The research mainly focuses on plant communities and vegetation succession in relation to lake level changes. We were informed that about 50 different types of plants, which are distributed in nearly concentric zones around the inner thermokarst lake, can be found between the lake and the surrounding taiga forest. The different vegetation zones are developing in dependence on differing soil-moisture conditions. In contrast to the forest distribution around the alases on the *Abalakh* terrace, the forest here is covering the alas slopes completely as well as the edges of the alas bottom. This can be explained by comparably coarser-grained sediments of the *Tyungyulyu* terrace, which facilitates the water uptake by the trees. The measured active layer depth within the alas were 1.20 m at the lake shore and 0.80 m under forest. Lake level changes in the *Ulakhan Sekhan* alas, monitored since many years by the Russian research group, can be seen exemplary for all thermokarst lakes in the region as lake level changes are mainly related to annual changes in precipitation. For example, lowest lake levels were explored around 2001. The lakes show highest level around 2006/2007 in relation to high annual precipitation. Since then, the explored thermokarst lake levels are decreasing again.
Finally, three other sites were visited at the end of the journey around *Ulakhan Sekhan*. The alas at the site Des2_Pingo (see Fig. 2.2C) contains a pingo. At the top of this pingo, dark grayish-black sediments contain huge amount of aquatic fauna (e.g. aquatic gastropods molluscs). However, the evolution of the pingo and this alas is still unclear. Surface-sediment samples were taken for preliminary analyses and ^{14}C dating. The pingo is showing indication for initial degradation. The active layer at the top was measured to be 1.50 m. The alas *Yunakh* (Des3 in Fig. 2.2C) was visited as another typical example for thermokarst processes on the *Tyungyulyu* terrace. The *Yunakh* alas is characterized by a typical vegetation zonation around the centred thermokarst lake (Fig. 2.11). At the end, a thermokarst lake in the *Tympa* stage was explored at the site DesJ4 (see Fig. 2.2C). This initial thermokarst lake was anthropogenically induced after agricultural usage of this area until the 1930s. The lake dealt as a research object for methane and carbon balancing by e.g. Desyatkin et al. [2009].

Fig. 2.11: *Panoramic view on the Yunakh alas (Des3 in Fig. 2.2C). This alas is a typical example for thermokarst on the Tyungyulyu terrace.*

2.5. Conclusions and Future Prospects

As we could see at many sites, the permafrost region in Central Yakutia responds very sensitive to environmental changes. The highly diverse thermokarst landscape in the Lena-Aldan-Amga region is thus very interesting from a scientific point of view and has a huge potential for research. Despite the decades-long and extensive knowledge of the Russian colleagues, many questions about the highly dynamical permafrost landscapes in Central Yakutia are still unanswered. This initiation trip was very helpful to get first insights in subarctic thermokarst processes in eastern Siberia and to get an idea of the logistical needs to conduct the proposed project. Future field work will focus locally on the *Yukechi* and the *Khara Bulgunakh* alases as both sites can be seen characteristically for thermokarst processes on the different geomorphological terraces. The field work will be combined regionally with remote sensing analyses. The goal will be the reconstruction of Holocene and recent permafrost degradation processes, their influencing factors and environmental impacts and based on that the assessment of future landscape evolution.

Acknowledgements

We would like to thank the technical and scientific assistant of all Russian colleagues involved in the impressive and successful exploration journey. The financial support of the Alfred Wegener Institute for Polar and Marine Research and the Melnikov Permafrost Institute Yakutsk to conduct the field trip is highly appreciated.

References

Desyatkin A.R., F. Takakai, P.P. Fedorov, M.C. Nikolaeva, R.V. Desyatkin and R. Hatano (2009). CH_4 emission from different stages of thermokarst in Central Yakutia, Eastern Siberia. Soil Science and Plant Nutrition, 55(4): 558-570.

Desyatkin, R.V. (2008). Soil formation in thermokarst depressions – Alases of Cryolithozone. Novosibirsk: Nauka, 324pp. (in Russian).

Fedorov, A.N. and P.Ya. Konstantinov, P.Ya. (2003). Observation of surface dynamics with thermokarst initiation, Yukechi site, Central Yakutia. Permafrost: Proceedings of the 8th International Conference on Permafrost, 21-25 July 2003, Zürich, Switzerland, 239-243.

Fedorov, A.N. and P.Ya. Konstantinov (2009). Response of permafrost landscapes of Central Yakutia to current changes of climate, and anthropogenic impacts. Geograph. Nat. Resour., 30. 146-150.

Grosse, G., J. Harden, M. Turetsky, A.D. McGuire, P. Camill, C. Tarnocai, S. Frolking, E.A.G. Schuur, T. Jorgenson, S. Marchenko, V. Romanovsky., K.P. Wickland, N. French, M. Waldrop, L. Bourgeau-Chavez and R.G. Striegl, (2011). Vulnerability of high latitude soil carbon in North America to disturbance, J. Geophys. Res., 116, G00K06, doi:10.1029/2010JG001507.

Jones, M. C., G. Grosse, B.M. Jones and K. Walter Anthony (2012). Peat accumulation in drained thermokarst lake basins in continuous, ice-rich permafrost, northern Seward Peninsula, Alaska. J. Geophys. Res., 117, G00M07, doi:10.1029/2011JG001766.

Matveev, I.A. (Ed.) (1989). Agricultural Atlas of the Republic Sakha (Yakutia). Nauka, Moscow, 115 pp. (in Russian).

Morgenstern, A., G. Grosse, F. Günther, I. Fedorova, and L. Schirrmeister (2011). Spatial analyses of thermokarst lakes and basins in Yedoma landscapes of the Lena Delta. The Cryosphere 5, 849-867.

Romanovsky, V.E., S.L. Smith, V.T., and H.H. Christiansen (2010). Permafrost Thermal State in the Polar Northern Hemisphere during the International Polar Year 2007–2009: a Synthesis. Permafrost Perigla. Proc., 21, 106-116.

Sazonova, T.S., V.E. Romanovsky, J.E. Walsh and D.O. Sergueev (2004). Permafrost dynamics in the 20th and 21th centuries along the East Siberian transect. J. Geophys. Res.109, D01108.

Soloviev, P.A. (1973). Thermokarst phenomena and landforms due to frostheaving in Central Yakutia. Biuletyn Peryglacjalny, 23, 135 – 155.

Walter, K.M., S. Zimov, J.P. Chanton, D. Verbyla, and F.S. Chapin III (2006). Methane bubbling from Siberian thaw lakes as a positive feedback to climate warming, Nature 443, 71–75.

3. EXPEDITION EYESIGHT-NAAT-ALASKA 2012

Marcel Buchhorn, Marcel Schwieder

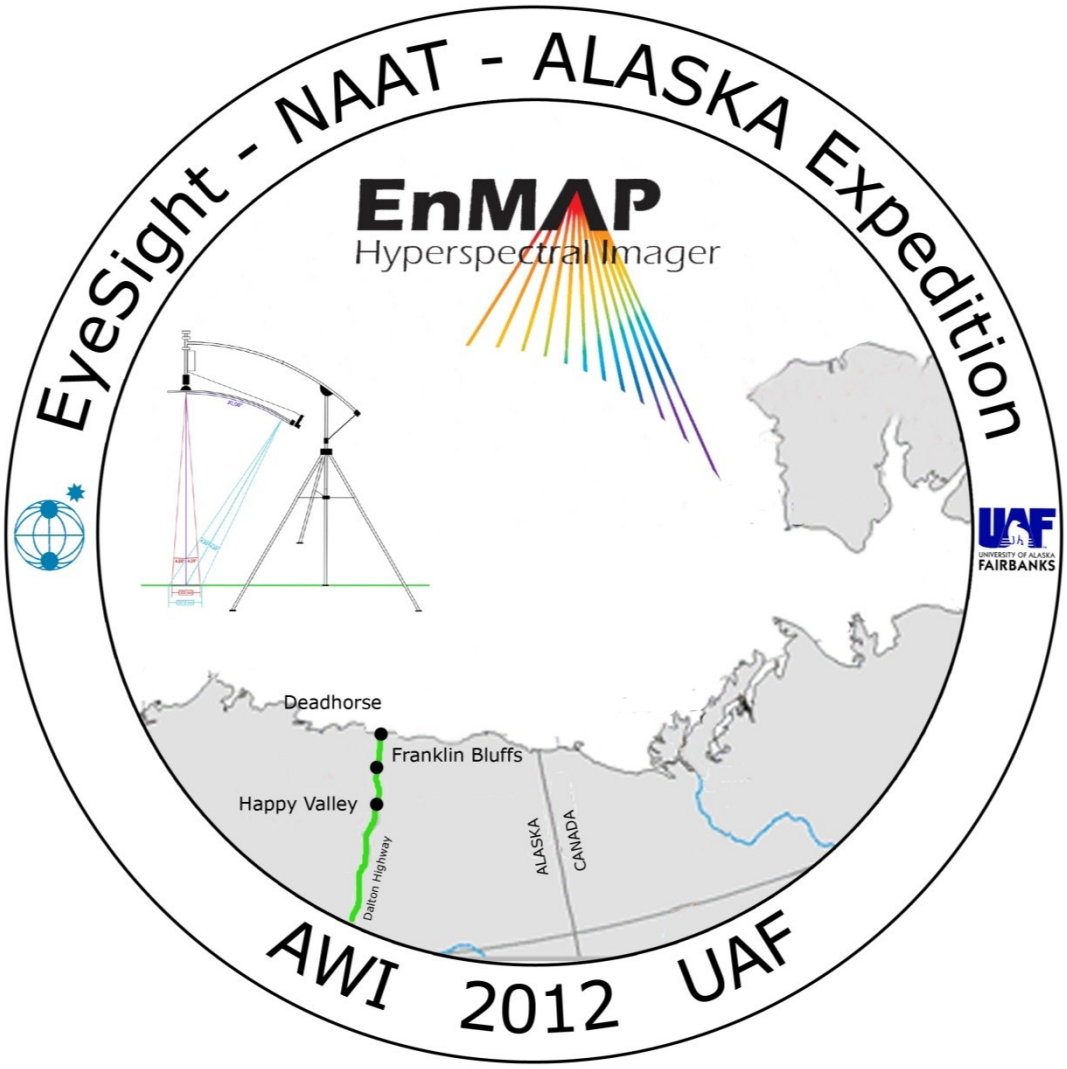

June 21 – July 22, 2012

North Slope, Alaska, USA

3.1. Introduction

Background and Objectives

Fieldwork on the Alaskan North Slope along the Low Arctic part of the North American Arctic Transect (NAAT), Alaska, USA, was undertaken in summer 2012. The expedition was carried out in cooperation with the Alaska Geobotany Center (AGC) of the University of Alaska Fairbanks (UAF).

Background of the expedition is the fact that climate-induced changes appear in high-latitude permafrost regions firstly in the change of surface temperature and moisture regimes. Secondarily, the changes appear on the vegetation coverage and vegetation development [Epstein et al., 2012]. These changes can be monitored through vegetation indices (VI) calculated from remote sensing data. The Alfred Wegener Institute (AWI) is integrated within the research project "hy-ARK-VEG" (hyperspectral method development for Arctic Vegetation biomes) in the mission preparation of the German, hyper-spectral "Environmental Mapping and Analysis Program" (EnMAP) satellite mission. The EnMAP mission will provide high-quality hyperspectral data at high temporal resolution for the monitoring of geophysical and biophysical parameters of the Earth's surface [Stuffler et al., 2007]. The start of EnMAP is planned for 2015. A major part of the project ‘hy-Arc-VEG’ focuses on spectro-radiometrical field measurements of a wide range of different tundra surface characteristics (vegetation, vegetation structure, moisture regimes) to technically explore the potential of multispectral- to hyperspectral satellite data in respect to the low-growing tundra biomes. Remote sensing algorithms for tundra adapted VI’s are developed based on the spectral field measurements. Moreover, questions about the influence of the BRDF (Bidirectional Reflectance Distribution Function) effect on these VI have to be answered. The BRDF gives the reflectance of a target as a function of illumination geometry and viewing geometry [Nicodemus et al., 1977]. In remote sensing, information about this effect is needed for the correction of view and illumination angle effects (for example in image standardization and mosaicking), for atmospheric correction and many more other applications.

In order to undertake such research a large data base of spectro-radiometric and BRDF field measurements of various arctic tundra biomes and well described study sites is needed. The EyeSight-NAAT-Alaska 2012 expedition follows up the data collection of the ECI-GOA-Yamal 2011 expedition, which took place in summer 2011 in Yamal, West Siberia, Russia. The AGC provides with the North American Arctic Transect (NAAT) a network of study sites that represents the full range of typical vegetation types in the North American Low Arctic.

The main research goals of the expedition were:

(i) to update the vegetation description of the established study sites;
(ii) the collection of spectro-radiometrical data of tundra biomes along environmental gradients to investigate remote sensing algorithms for spectral narrow-band and broad-band vegetation indices (VI);
(iii) anisotropy (BRDF) studies on spectral reflectance of the main plant communities using an in-house (at AWI) developed field spectro-goniometer.

Expedition Itinerary and General Logistics

The expedition team consisted of one participant from the Humboldt Universität zu Berlin (HU Berlin) and one from the Alfred Wegener Institute for Polar and Marine Research (AWI Potsdam) (Fig. 3.1 and Tab. 3.1).

Fig. 3.1: *Participants from left to right: Marcel Buchhorn (AWI), Marcel Schwieder (HU Berlin)*

To access the study sites, a Dodge Ram 2500 camper truck was used (Fig. 3.2). This truck was our home during the whole expedition and brought us from Fairbanks up to Prudhoe Bay and back (overall more than 1,600 km). Since all study sites are along the Dalton Highway, we had the chance to camp directly next to the study sites (Fig. 3.3).

Fig. 3.2: *Expedition vehicle and home. Pictures by M. Schwieder and M. Buchhorn*

Tab. 3.1: *Participants of the expedition EyeSight-NAAT-ALASKA 2012 (in alphabetical order)*

Participant	Organisation/Institute	E-mail
Buchhorn, Marcel (expedition leader)	Alfred Wegener Institute	Marcel.Buchhorn@awi.de
Schwieder, Marcel	Humboldt-Universität zu Berlin	Marcel.Schwieder@geo.hu-berlin.de

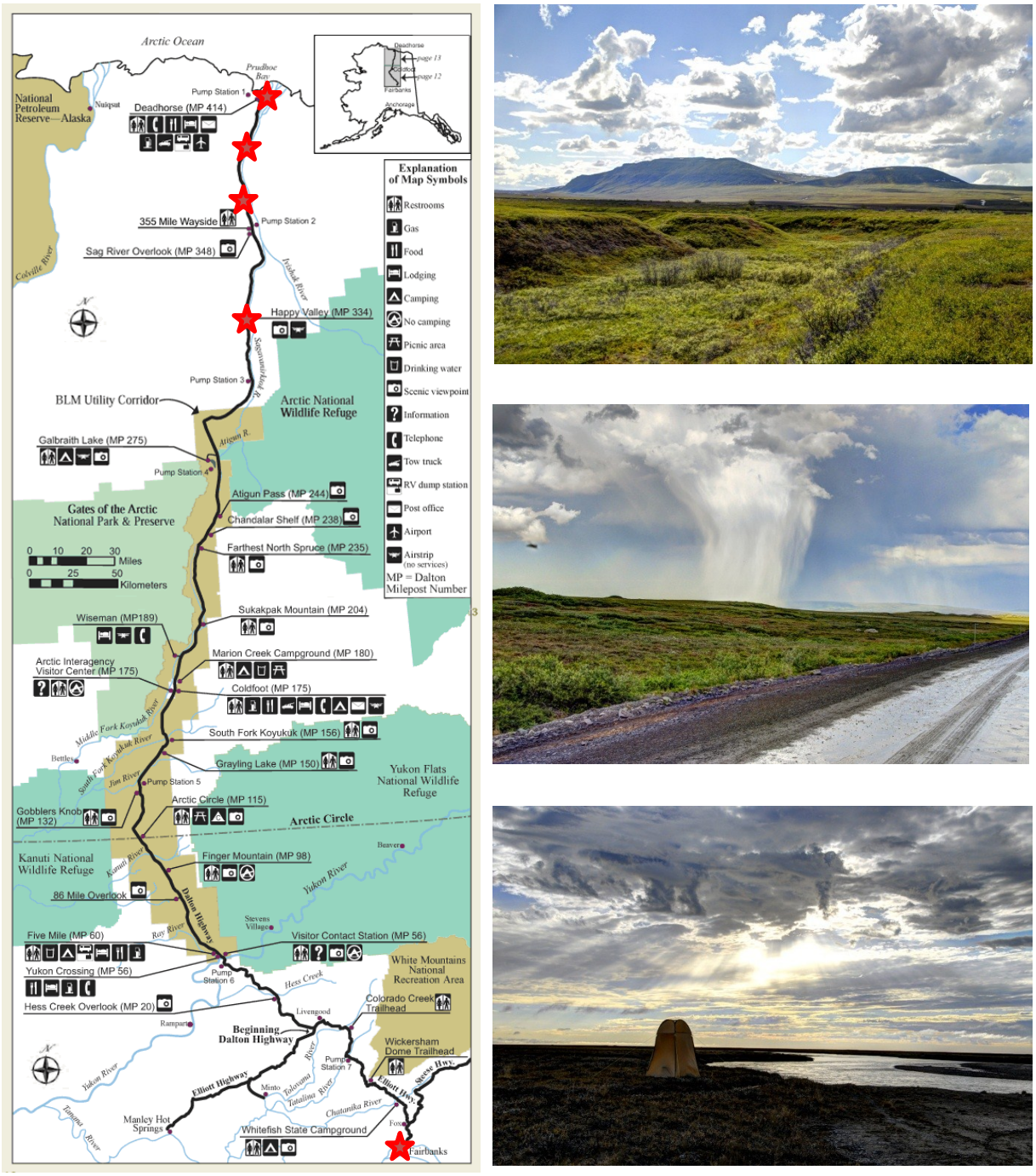

Fig. 3.3: *left: expedition route (Fairbanks to Deadhorse along the Elliot and Dalton Highway). Image from BLM.gov, public domain, PD-USGov-BLM. Right: expedition impressions. Pictures by M. Buchhorn.*

The field work started on June 25th and was completed on July 17th. The days before and after where used for expedition preparation and wrap-up. The itinerary of the expedition is shown in Tab 2 (a more detailed overview about the itinerary can be found in Annex Tab. A.1.2).

Tab. 3.2: *Time table for the EyeSight-NAAT-ALASKA 2012 expedition*

Date	Location	Task
21. & 22.06.2012	Fairbanks	Preparation of the expedition and the truck
23. & 24.06.2012	Fairbanks, Coldfoot, Toolik Field Station, Happy Valley	Departure from Fairbanks to study area "Happy Valley" via Elliot and Dalton Highway over Coldfoot and Toolik Field Station
25.06.-05.07.2012	Happy Valley	Field work
04.07.2012	Sagwon	Field work (day trip but main camp in Happy Valley)
05.07.2012	Happy Valley, Franklin Bluffs	Move to the next study area
06.-15.07.2012	Franklin Bluffs	Field work
11. & 12.07.2012	Deadhorse	Field work (two day trip but main camp in Franklin Bluffs)
15.07.2012	Franklin Bluffs, Happy Valley	Move back to first study area
16.-18.07.2012	Happy Valley	Field work
18. & 19.07.2012	Happy Valley, Toolik Field Station, Coldfoot, Fairbanks	Departure from study area "Happy Valley" to Fairbanks via Dalton and Elliot Highway over Toolik Field Station and Coldfoot
20.-22.07.2012	Fairbanks	Expedition wrap-up (equipment cleaning)

Fig. 3.4: *Pass of the Arctic Circle on June 23th, 2012. Picture by M. Buchhorn and M. Schwieder.*

Study Sites

The CAVM (Circumpolar Arctic Vegetation Map) divide the Arctic into five bioclimate subzones (A-E, cold to warm). The Low Arctic is defined by subzones D and E [Walker et al., 2005]. The North American Arctic Transect (NAAT), established in 2001–2006, follows the road network of the Dalton Highway. The four study areas on this expedition - Deadhorse (transition zone C/D), Franklin Bluffs, Sagwon Hills (transition zone D/E), and Happy Valley (Subzone E) - are established at the 250 km Low Arctic part of this transect. All study areas contain one to three homogeneous study sites, which mean that overall nine study sites have been visited during the EyeSight-NAAT-ALASKA expedition (Fig. 3.5).

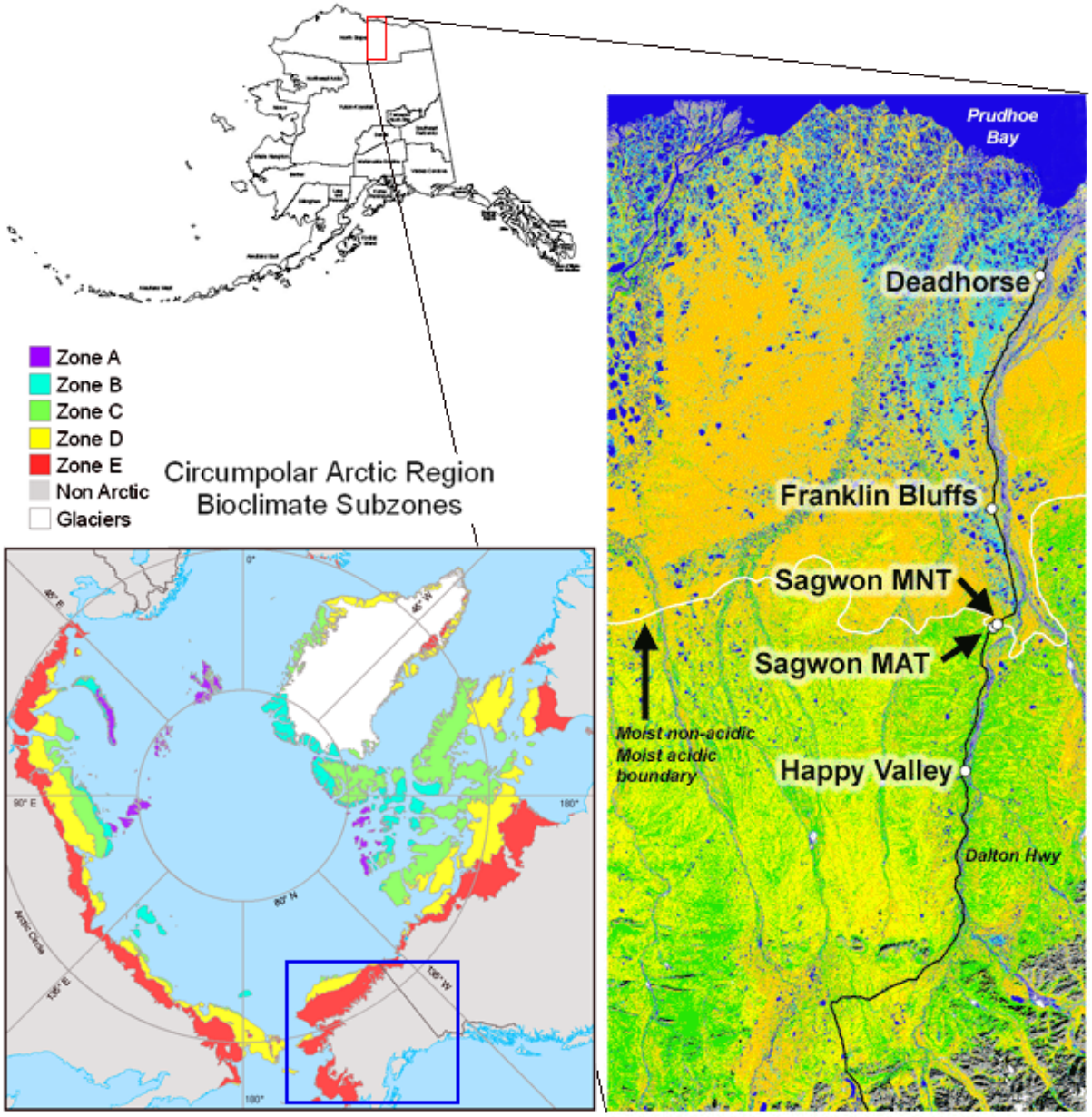

Fig. 3.5: *Location of the study sites. The down left box shows the CAVM with the five bioclimate subzones. Note the blue rectangle which marks Alaska. The right box shows the four Low Arctic study areas. Images by AGC and Walker et al. [2005].*

A detailed description of the flora and geology of the Low Arctic part of the NAAT can be found in Kade et al. [2005] and for the High Arctic part in Vonlanthen et al. [2008]. Walker et al. [2011] give the most recent overview about the research work along the NAAT, which include a synthesis of various publications addressing biocomplexity in arctic regions [Walker et al., 2008a].
All nine test sites are homogeneous 10x10 m grids and represent the typical vegetation along environmental gradients (soil moisture, pH-value, toposequence, regional climate). The soil moisture gradient is represented by the three test sites in the Franklin Bluffs study area (FB_dry, FB_zonal, FB_wet) (Fig. 3.11-3.13), where the toposequence is represented by the three test sites at Happy Valley (HV_footslope, HV_midslope, HV_hillcrest) (Fig. 3.6-3.8). The two test sites at Sagwon form the transition from the acidic to the non-acidic tundra (SW_MAT, SW_MNT) (Fig. 3.9-3.10). The five zonal sites of all study areas (HV_midslope, SW_MAT, SW_MNT, FB_zonal, DH_zonal) (Fig. 3.7, 3.9, 3.10, 3.12, 3.14) show the temperature changes from south to north, which describes the regional climate gradient. In Tab. 3.3 the main characteristics of the test sites are shown, where Fig. 3.6 to 3.14 gives an impression of the sites.

Fig. 3.6: *The Happy Valley footslope (HV_footslope) study site. Life form description: moist tussock graminoid, erect dwarf-shrub, moss tundra. Picture by M. Buchhorn.*

Fig. 3.7: *The Happy Valley midslope (HV_midslope) study site. Life form description: moist tussock graminoid, erect dwarf-shrub, moss tundra. Picture by M. Buchhorn.*

Fig. 3.8: *The Happy Valley hill crest (HV_hillcrest) study site. Life form description: moist tussock graminoid, erect dwarf-shrub, moss tundra. Picture by M. Buchhorn.*

The Happy Valley study area (subzone E) (Fig. 3.6-3.8) is located on a gentle west-facing slope in the foothills of the Brooks Range. The study sites are located at the hill crest (325 m), one at the footslope (300 m), and the zonal site is representing also the midslope (310 m) site. All three sites are characterised by moist acidic tundra (MAT) vegetation communities (moist tussock graminoid, erect dwarf-shrub, moss tundra), whereas the height and area coverage of dwarf-shrubs is increasing from the hill crest to the footslope. The Happy Valley study area is important, since all typical vegetation communities of MAT are located within a small area.

The Sagwon study area (transition zone D/E) (Fig. 3.9 & 3.10) is located in the transition between the foothills and the coastal plain. Due to difference in the substrate this area represents also the boundary between the moist acidic tundra (MAT) and moist non-acidic tundra (MNT). This two tundra types have complete different vegetation communities.

Fig. 3.9: *The Sagwon MAT (SW_MAT) study site (MAT = moist acidic tundra). Life form description: moist tussock graminoid, erect dwarf-shrub, moss tundra. Picture by M. Buchhorn.*

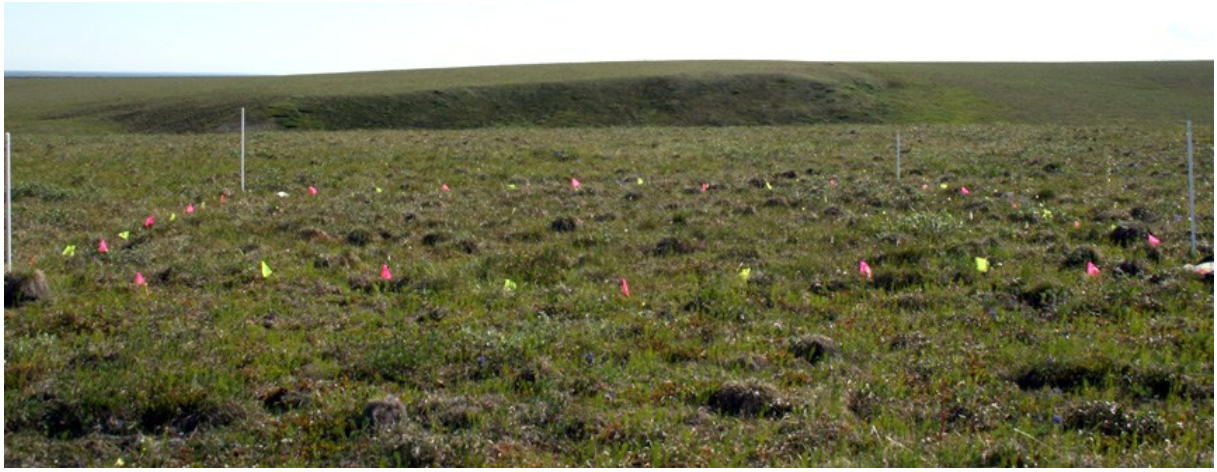

Fig. 3.10: *The Sagwon MNT (SW_MNT) study site (MNT = moist non-acidic tundra). Life form description: moist graminoid, sedge, prostate dwarf-shrub tundra. Picture by M. Buchhorn.*

The Franklin Bluffs study area (subzone D) (Fig. 3.11-3.13) is located in the coastal plain on a flat, low old terrace of the Sagavanirktok River. All three sites are characterised by moist non-acidic tundra (MAT) vegetation communities (sedge dominated, prostate dwarf-shrubs). The main difference of the test sites is the soil moisture content (wet to dry) which is important for the vegetation development. Analysis of this gradient is important in various remote sensing applications.

The Deadhorse study area (transition zone C/D) (Fig. 3.14) is located in the coastal plain near the Arctic Ocean. It is characterized by MAT. The site is very wet, but represents the zonal vegetation in this area. Together with the zonal test sites from Happy Valley, Franklin Bluffs and Sagwon a regional climate gradient can be analysed.

Fig. 3.11: *The Franklin Bluffs wet (FB_wet) study site. Life form description: wet graminoid-moss tundra; sedge dominated. Picture by M. Buchhorn.*

Fig. 3.12: *The Franklin Bluffs zonal (FB_zonal) study site. Life form description: moist graminoid, sedge, prostate dwarf-shrub tundra. Picture by M. Buchhorn.*

Fig. 3.13: *The Franklin Bluffs dry (FB_dry) study site. Life form description: dry prostate dwarf-shrub, lichen tundra; sedge dominated. Picture by M. Buchhorn.*

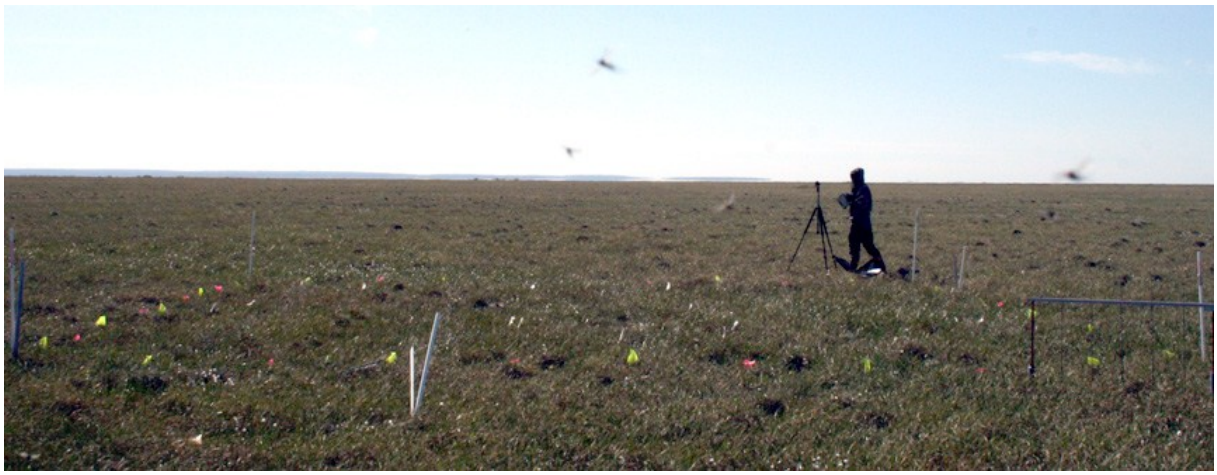

Fig. 3.14: *The Deadhorse zonal (DH_zonal) study site. Life form description: moist graminoid, sedge, prostate dwarf-shrub tundra. Picture by M. Buchhorn.*

Tab. 3.3: *Main characteristics of the nine test sites; data from Raynolds et al. [2008]*

Location	Grid Name	Latitude Longitude	SWI, °C	Bioclimate Subzone	Topography	Land Cover	Dominant Type of Patterned Ground	Soil
Deadhorse	DH-zonal	70° 09′ 42″ N 148° 27′ 49″ W	17.3	D	Flat	Sedge dominated with prostrate dwarf shrubs on higher (drier) microsites	Medium-size nonsorted circles	Coarse-silty, mixed, active, pergelic Typic Aquiturbel
Franklin Bluffs	FB-dry	69° 40′ 29″ N 148° 43′ 15″ W	24.2	D	Flat	Sedge dominated with prostrate dwarf shrubs and lichens on higher (drier) microsites	Medium-size nonsorted circles	Silty, mixed, superactive, supergelic Ruptic-Histic Aquiturbel
	FB-zonal	69° 40′ 28″ N 148° 43′ 16″ W	24.2	D	Flat	Sedge dominated with prostrate dwarf shrubs and lichens on higher (drier) microsites	Medium-size nonsorted circles	Silty, mixed, superactive, supergelic Ruptic-Histic Aquiturbel
	FB-wet	69° 40′ 27″ N 148° 43′ 01″ W	24.2	D	Flat	Wet sedge vegetation with drier rims, wetter troughs, and large boils with cryptogamic crust	Large nonsorted circles	Coarse loamy over sandy, mixed superactive, supergelic Aquic Haploturbel
Sagwon Nonacidic	SN-zonal	69° 26′ 01″ N 148° 40′ 18″ W	26.5	D	Hill crest	Sedge dominated with prostrate dwarf shrubs and lichens on higher (drier) microsites	Small nonsorted circles	Coarse-silty, mixed, superactive, supergelic Aquic Ochreturbel
Sagwon Acidic	SA-zonal	69° 25′ 33″ N 148° 41′ 34″ W	26.5	E	Hillslope	Tussock-sedge with erect dwarf shrubs	Small nonsorted circles	Coarse-silty, mixed, superactive, hypergelic Ruptic-Histic Aquiturbel
Happy Valley	HV-dry	69° 08′ 49″ N 148° 51′ 08″ W	29.5	E	Top of slope	Tussock-sedge with erect dwarf shrubs	Small nonsorted circles	Coarse-silty, mixed, superactive, pergelic Ruptic-Histic Aquiturbel
	HV-zonal	69° 08′ 48″ N 148° 50′ 54″ W	29.5	E	Hillslope	Tussock-sedge with erect dwarf shrubs	Small nonsorted circles	Coarse-silty, mixed, superactive, pergelic Ruptic-Histic Aquiturbel
	HV-mesic	69° 08′ 50″ N 148° 50′ 49″ W	29.5	E	Toe of slope	Tussock-sedge with erect dwarf shrubs	Small nonsorted circles	Coarse-silty, mixed, superactive, pergelic Ruptic-Histic Aquiturbel

[a]SWI, summer warmth index, the sum of monthly means >0°C

3.2. Spectro-Radiometrical Characteristics of Low-Growing Tundra Plant Communities

Field Work & Methods

The spectral reflectance signature of an object (spectro-radiometric properties), a function of reflectance over wavelength, are determined by the physical and chemical properties of this object [Jakomulska et al., 2003]. For plants this properties can be grouped in regions of the electromagnetic spectrum. The visible region (400 to 700 nm) is mainly influenced by the pigment content of the plant, whereas the near infrared (NiR) region (700 to 1400 nm) is mainly affected by plant cell structure.
For the spectro-radiometric characterisation of the main Low Arctic vegetation communities each grid of 10x10 m was subdivided into 100 plots. In each plot the spectral signature was measured with a field spectrometer and all signatures have been averaged in order to provide one spectral response curve representing the test site. These averaged signatures are used for all further calculations and comparisons.
We used two portable GER® 1500 field spectrometers (350-1050nm) provided by the GFZ (German Research Centre for Geosciences). For the standard measurements, one GER was equipped with a 4° Field-Of-View (FOV) fore-optic for the radiance measurements and the other GER with a cosine diffuser optic for the irradiance measurement (Fig. 3.15).

Fig. 3.15: *Set-up for the spectro-radiometric measurements (here: device check). Left: irradiance measurement; Right: radiance measurement of the target (simultaneously with the irradiance measurement). Pictures by M. Buchhorn and M. Schwieder.*

In order to describe the vegetation characteristics we used the Braun-Blanquet approach [Dierschke, 1994]. The average soil-moisture content was calculated from point measurements with a TDR (Time Domain Reflectrometry) soil moisture meter. Each plot was also photographed and for the whole sites 360° panorama photos in the visible as well as near-infrared spectra have been produced. A detailed overview about all field work and samples can be seen in Annex A1.

Using the formulas 1, 2 and 3 the following indices were calculated from the field spectrometer measurements:

- the spectral surface reflectance coefficient R(λ) from 400 nm to 900 nm (due to moisture-related noise the wavelengths > 900 nm were removed)
- sensor-specific Normalized Differenced Vegetation Indices (NDVI):
  multi-spectrally based indices (broad-band indices): NDVI AVHRR, NDVI MODIS (multi-spectral land mode), NDVI Landsat, NDVI SPOT, NDVI GEOEye, NDVI QuickBird;
  super-spectrally based indices (high-spectral resolution band indices): NDVI MODIS (super-spectral water mode), NDVI MERIS;
  hyper-spectrally based indices (hyper-spectral resolution band indices): NDVI EnMAP, NDVI CHRIS/PROBA, NDVI Hyperion, NDVI field spectro-radiometry (single wavelengths-based with 1.5 nm spectral resolution);
- Fraction of Absorbed Photosynthetically Active Radiation (fAPAR) for different Tundra biomes as well as algorithms for Leaf-Area-Index (LAI) derivatives from fAPAR.

The spectral reflectance coefficient, R(λ), is calculated as

$$R(\lambda) = \frac{L_{up}(\lambda)}{L_{in}(\lambda)} \quad (1)$$

R= reflectance [dimensionless]; x 100 [%]
L_{in}= incoming (downwelling) radiance [W m^{-2} sr^{-1} nm^{-1}] (measured back-reflected from the Spectralon© reference plate and interpolated to the time of the target measurement via irradiance)
L_{up}= upwelling radiance [W m^{-2} sr^{-1} nm^{-1}] (measured back-reflected from the surface/target)

The Normalized Differenced Vegetation Indix (NDVI) is calculated as

$$NDVI = \frac{R_{NIR} - R_{red}}{R_{NIR} + R_{red}} \quad (2)$$

NDVI= Normalized Differenced Vegetation Indices
R_{NIR}= reflectance within the Near InfraRed, NIR, wavelength band
R_{red}= reflectance within the red wavelength band

The used wavelengths for the NDVI calculation of the AVHRR, MODIS and EnMAP sensors are:

	MODIS	AVHRR	EnMAP
RED	620-670nm	580-680nm	672nm
NIR	841-876nm	725-1000nm	840nm

In case of 100% vegetation coverage, the fraction of Absorbed Photosynthetically Active Radiation, fAPAR, can be calculated as

$$fAPAR = \frac{\sum_{\lambda=400nm}^{700nm}[\pi \cdot L_{in}] - \sum_{\lambda=400nm}^{700nm}[\pi \cdot L_{up}]}{\sum_{\lambda=400nm}^{700nm}[\pi \cdot L_{in}]} \quad (3)$$

fAPAR= fraction of Absorbed Photosynthetically Active Radiation
L_{in}= incoming (downwelling) radiance [W m^{-2} sr^{-1} nm^{-1}] (measured back-reflected from the Spectralon© reference plate) ***or*** measured directly as incoming (downwelling) irradiance, E_{in}, [W m^{-2} nm^{-1}] with the cosine diffuser, then use $\sum_{\lambda=400nm}^{700nm} E_{in}$ instead of $\sum_{\lambda=400nm}^{700nm} (\pi \cdot L_{in})$
L_{up}= upwelling radiance [W m^{-2} sr^{-1} nm^{-1}] (measured back-reflected from the surface/target)

Preliminary Results

The average reflectance spectra of the nine sites show low reflectance peaks in the green wavelength range, low absorption depths in the red wavelength band and smooth Near InfraRed (NIR) reflectance shoulders (see Annex A2). This observation confirms a reflectance type that is caused by the low multiple scattering activities in the NIR that is typical for a low-growing vegetation structure. The green reflectance peak seems to be degraded due to absorption by carotinoides and anthocanides in the greenish-to red wavelength range. This range has no effect on the NDVI or similar VI derived from the broad red and the NIR wavelength range. Fig. 3.16 shows the spectral signature of typical Low Arctic vegetation communities. In order to show the influence of the vegetation community on the behaviour of the average spectral response, pure spectral signatures of plant species (endmember) are added in the graph.

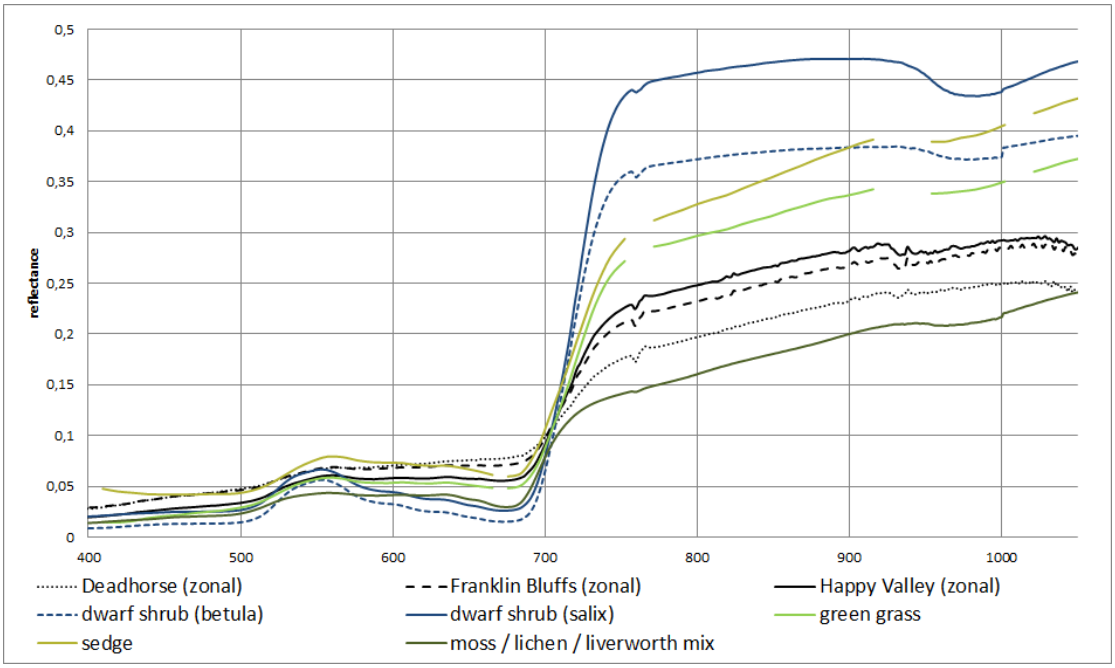

Fig. 3.16: *Comparison of spectral signatures of typical low-growing Low Arctic vegetation communities and spectral signatures of pure plant species.*

However, tundra-specific reflectance types result always in a range of low NDVI values due to low scattering activities in the NIR (see Annex A3). This behaviour is already reported in earlier publications. Nevertheless, new information regarding spectral reflectance of acidic and nonacidic tundra in the visible blue region could be helpful for determining the mechanisms responsible for the striking spectral separation of these vegetation types noted during earlier studies at plot- to circumpolar spatial scales.

3.3. BRDF characteristics of low-growing Tundra plant communities

Field Work & Methods

Spectro-radiometrical multi-zenith and multi-azimuth measurements simulate the viewing geometries of wide-angle looking satellite sensors such as AVHRR, MODIS, MERIS or sensors with technical side-looking possibilities such as the EnMAP sensor. The Bidirectional Reflectance Distribution Function (BRDF) characteristics of low-growing tundra biomes have not been investigated in depth so far [Vierling et al., 1997]. BRDF gives the reflectance of a target as a function of illumination geometry and viewing geometry. Data on BRDF characteristics are needed for the correction of view and illumination angle effects of optical remote sensing data. A spectro-goniometer is a mechanical device for the spectro-radiometric measurement of the reflectance characteristics of a surface under a freely selectable angle of sensor azimuth (Φv) and sensor zenith (viewing angle) (θv) and at-site given ranges of angle of sun azimuth (Φs) and sun zenith (θs) (depending on latitude, longitude).

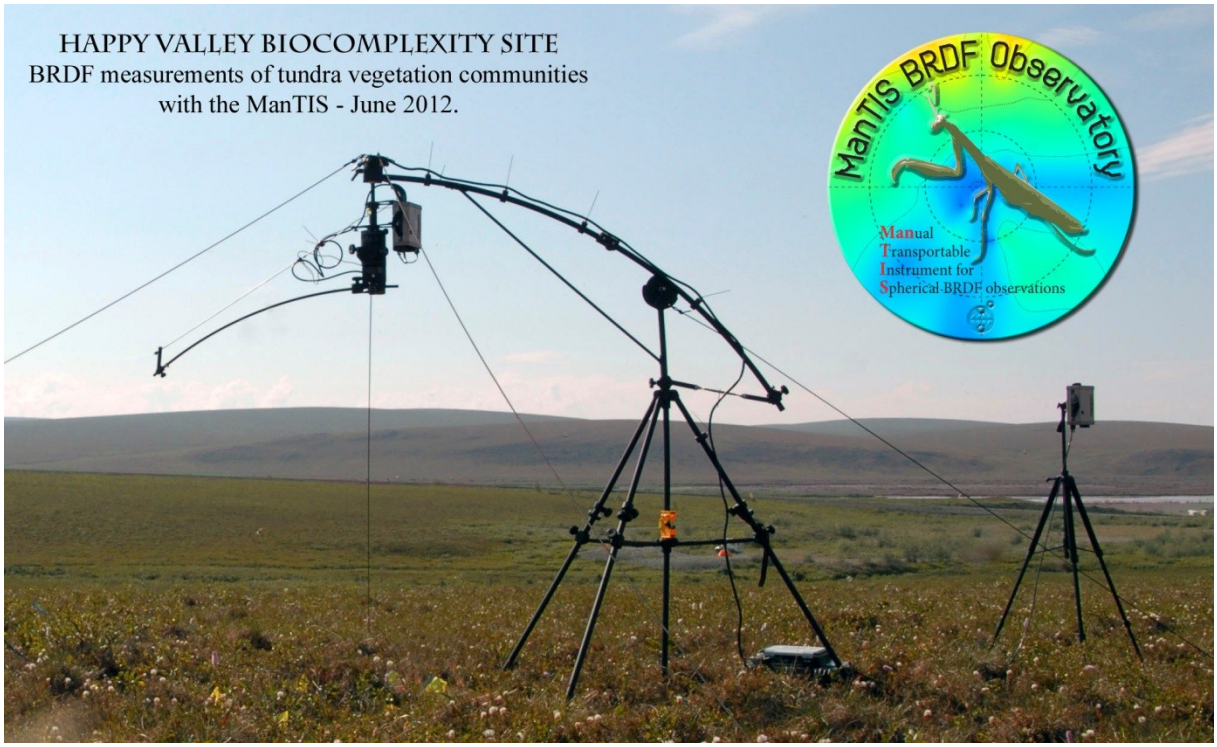

Fig. 3.17: *The ManTIS spectro-goniometer of the AWI. This transportable, field goniometer is the first of its kind and adapted to the Arctic environment. Picture by M. Buchhorn.*

Up to now, no suitable field goniometer for measurements in the Arctic was available. Within the “hy-ARC-VEG” project we designed a new, light-weight and transportable goniometer. The in-house (at AWI) developed and build field spectro-goniometer, named ManTIS (Manual Transportable Instrument for Spherical BRDF observations), was patented in 2011 and is equipped with the two GER1500 spectro-radiometers in the current set-up (Fig. 3.17). (Please note: The ManTIS instrument was formally known as EyeSight instrument. Due to trademark reasons the name was changed in 2012, but not in the expedition name.)

The ManTIS spectro-goniometer was first used at the Yamal expedition in 2011. The gained field experience was used for a design improvement in 2012. The spectrometer installed on the ManTIS spectro-goniometer measures the upwelling radiance [W m-2 sr-1 nm-1] of the surface (target). The optic of the spectrometer can be moved in circles around all the azimuth angles, and can be installed along the arc up to 30° sensor viewing angle. The reference measurements of a white reference Spectralon© plate is frequently made at the start and the end of each measurement cycle. In parallel, the second spectrometer installed on a tripod, continuously measures the downwelling irradiance [W m-2 nm-1] using a cosine diffuser installed on a 8° FOV fore-optic. The BRDF measurements can only be carried out during optimal sky conditions.

The Bidirectional Reflectance Factor, BRF, is calculated

$$BRF(\lambda,\theta_s,\phi_s,\theta_v,\phi_v) = \frac{\lfloor L_{up}(\lambda,\theta_s,\phi_s,\theta_v,\phi_v)(t_2)\rfloor(t_1)}{L_{in}(\lambda,\theta_s,\phi_s)(t_1)} \cdot R_{REF} \quad (4)$$

BRF= Bidirectional Reflectance Factor
L_{in}= incoming (downwelling) radiance [W m^{-2} sr^{-1} nm^{-1}] (measured back-reflected from the Spectralon© reference plate)
L_{up}= upwelling radiance [W m^{-2} sr^{-1} nm^{-1}] (measured back-reflected from the surface/target)
R_{REF}= Reflectance function of the Spectralon reference plate
[…](t) = stands for linear interpolation of bracket contents to time t
θ_s = sun zenith; Φ_s = sun azimuth; θ_v = sensor zenith; Φ_v = sensor azimuth;

The time interpolation ([…](t)) is needed in order to bring all measurements to the time of the upwelling measurement by using the irradiance measurement of a second spectrometer measurement.

$$L(x) = L(t) \cdot \frac{E(x)}{E(t)} \quad (5)$$

L = radiance [W m^{-2} sr^{-1} nm^{-1}]
E = irradiance [W m^{-2} nm^{-1}]
(x) = searched time stamp
(t) = given time stamp

A detailed overview about all field work and samples can be seen in Annex A1.

Preliminary Results

The first results of the BRDF analyses do not show the theoretical behaviour of the BRDF effect on homogeneous vegetated surfaces. The theoretical shape of the BRDF is that the maximum reflectance is displaced towards the backward scattering direction and the minimum reflectance towards the forward scattering direction (Fig. 3.18).

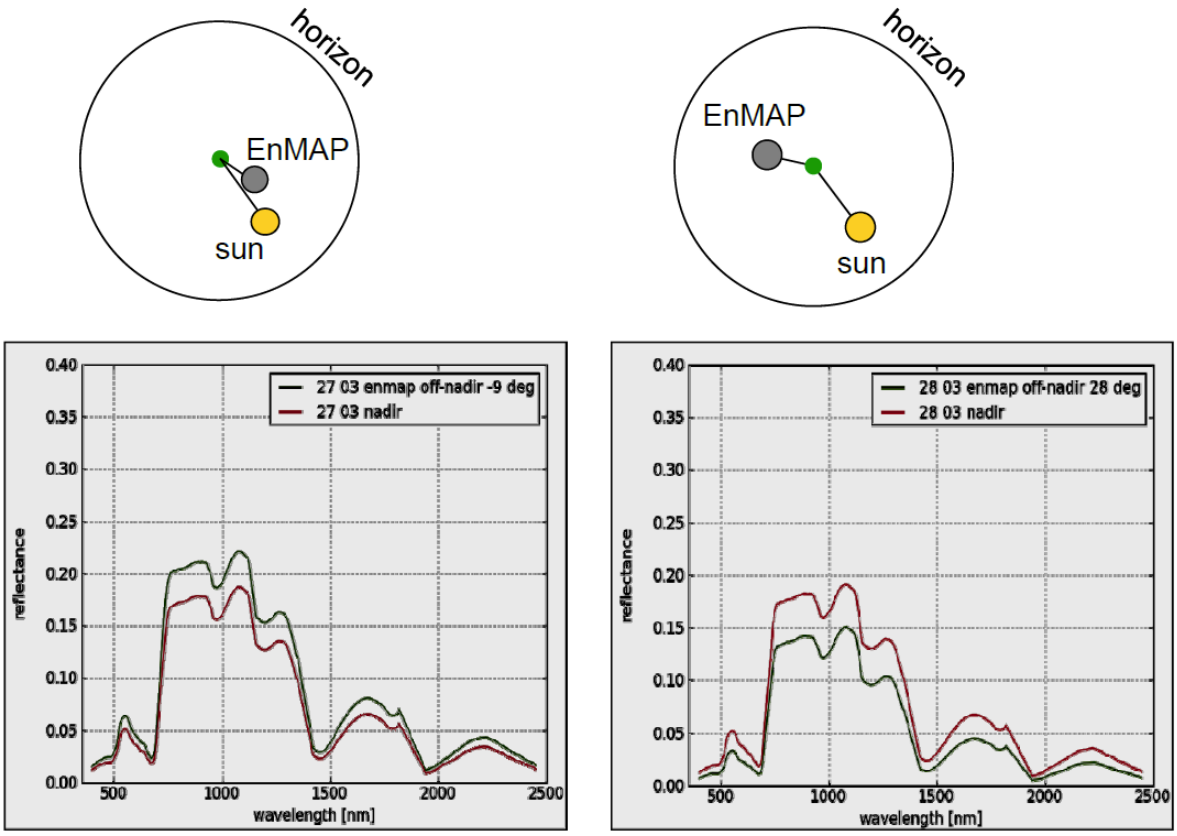

Fig. 3.18: *Theoretical behaviour of the BRDF effect. Left: Higher reflectance values of the sensor looking in the backward scattering direction (green curve) than looking nadir (red curve). Right: Lower reflectance values of the sensor looking in the forward scattering direction (green curve) than looking nadir (red curve).*

The first BRDF calculations for the tundra low-growing vegetation communities at the NAAT proof the mirror asymmetry in relative azimuth with respect to the principal plane. This behaviour was already seen in the BRDF analysis of the Yamal sites (ECI-GOA-Yamal 2011 expedition). Since not all BRDF spheres of this expedition has been yet analysed, the corresponding results of the Yamal expedition are used to explain the typical BRDF behaviour of Low Arctic plant communities.
The BRDF calculations show the maximum scattering displaced in the backward direction, but no minimal forward scattering. Instead, the forward scattering from the moss-dominated tundra type is characterised by similar to higher reflectance values in the forward scattering direction (see Fig. 3.19).

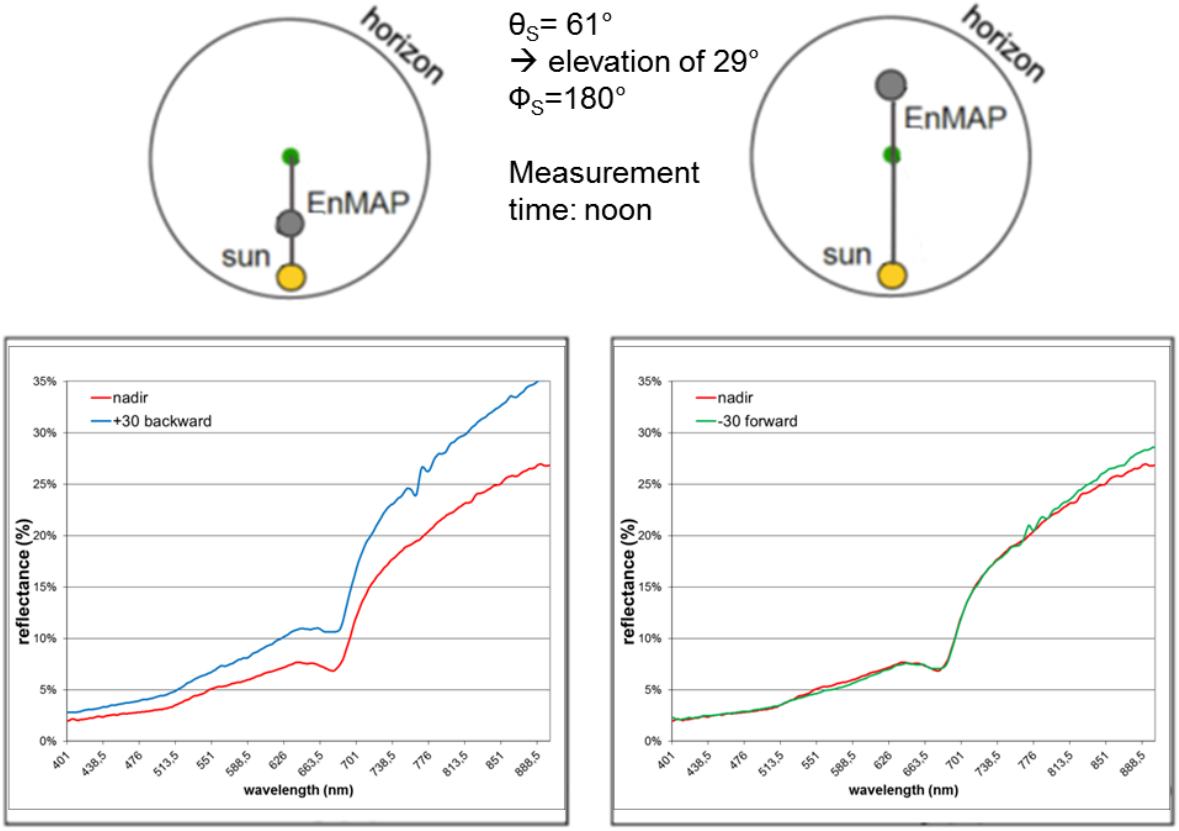

Fig. 3.19: *Behaviour of the BRDF effect in Low Arctic vegetation communities. Left: Higher reflectance values of the sensor looking in the backward scattering direction (blue curve) than looking nadir (red curve). Right: Equal reflectance values of the sensor looking in the forward scattering direction (green curve) and looking nadir (red curve). Note: result from plot 25, Vaskiny Dachi site 1, Yamal (2011-08-29).*

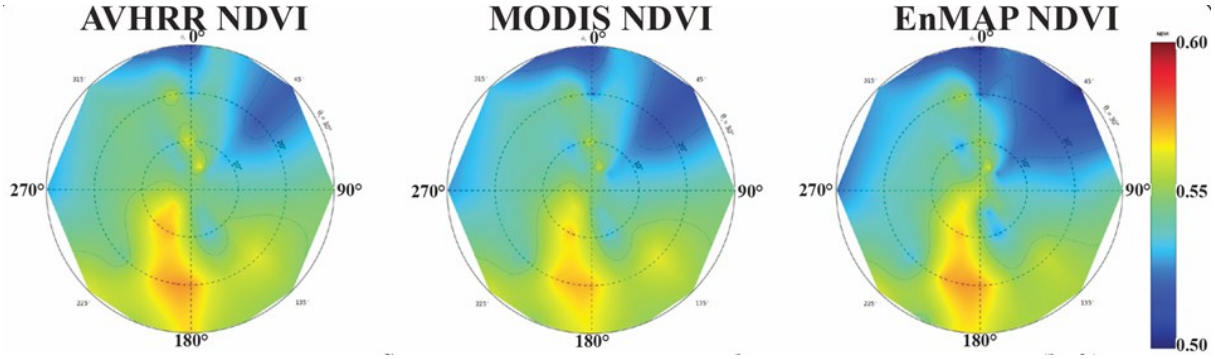

Fig. 3.20: *Behaviour of the BRDF effect on vegetation indices in Low Arctic vegetation communities (here: NDVI). Left: for the AVHRR satellite sensor. Middle: for the MODIS satellite sensor. Right: for the EnMAP satellite sensor.*

The 2-dimensional BRDF NDVI graphs (AVHRR NDVI, MODIS NDVI, EnMAP NDVI) show that the BRDF effect is also visible in the vegetation indices, which are calculated out of the reflectance values at specific wavelength bands (Fig. 3.20). The band width and center position of the RED- and NIR-sensor bands that are the input

bands into the NDVI calculation has only an influence on the absolute NDVI values, but the BRDF effect appears in all calculations with the same intensity.
The analysis show that the BRDF influence on VI‘s of low-growing arctic biomes has to be taken into account for the development of tundra-adapted VI‘s. The low sun zenith angles in the Arctic latitudes prevent hotspot-effects if the sensor viewing geometry is limited by the 30° sensor viewing angle and does not tilt further, but a BRDF normalization is still needed.

Acknowledgements

This work is part of the hy-ARK-VEG (hyperspectral method development for ARCtic VEGetation biomes) project sponsored by the German research center for aeronautics and space (DLR) and funded by the German Federal Ministry of Economics and Technology [support code: 50 EE 1013] in preparation of the EnMAP mission. Moreover, we want to thank the Helmholtz Graduate School for Polar and Marine Research (POLMAR) for funding an outgoing scholarship for a research stay at the Alaska Geobotany Center (AGC) at the University of Alaska Fairbanks.

List of Acronyms

AVHRR	Advanced Very High Resolution Radiometer
AWI	Alfred Wegener Institute for Polar and Marine Research
BRDF	Bidirectional Reflectance Distribution Function
BRF	bidirectional reflectance factor
ECI	Earth Cryosphere Institute
EnMAP	Environmental Mapping and Analysis Program
EyeSight	EnMAP-specific field spectro-goniometer (now called ManTIS)
fAPAR	fraction of Absorbed Photosynthetically Active Radiation
FOV	Field of View
GER	Spectrometer of the company SVC (Spectra Vista Corporation)
GFZ	German Research Centre for Geosciences Potsdam
hy-Arc-VEG	hyperspectral Arctic VEGetation Indices
LAI	Leaf Area Index
ManTIS	Manual Transportable Instrument for Spherical BRDF observations (former called EyeSight)
MERIS	Medium Resolution Imaging Specrometer
MODIS	Moderate-Resolution Imaging Spectroradiometer
NAAT	North American Arctic Transect
NDVI	Normalized Differenced Vegetation Indix
NIR	Near Infrared
VI	vegetation indices
θs = SZA	sun zenith angle
θv	sensor zenith
Φs = SAA	sun azimuth angle
Φv	sensor azimuth

References

Dierschke, H., 1994. Pflanzensoziologie: Grundlagen und Methoden : 55 Tabellen. Ulmer, Stuttgart, 683 S.

Epstein, H.E., Raynolds, M.K., Walker, D.A., Bhatt, U.S., Tucker, C.J., Pinzon, J.E., 2012. Dynamics of aboveground phytomass of the circumpolar Arctic tundra during the past three decades. Environ. Res. Lett 7 (1), 15506.

Jakomulska, A., Zagajewski, B., Sobczak, M., 2003. Field Remote Sensing Techniques for Mountains Vegetation Investigation, in: Proceedings of the 3rd EARSeL workshop on Imaging Spectroscopy. Herrsching, Germany, May 13th to 16th 2003, Herrsching, pp. 580–596.

Kade, A., Walker, D.A., Raynolds, M.K., 2005. Plant communities and soils in cryoturbated tundra along a bioclimate gradient in the Low Arctic, Alaska. Phytocoenologia 35 (4), 761–820.

Nicodemus, F.E., Richmond, J.C., Hsia, J.J., Ginsberg, I.W., Limperis, T., 1977. Geometrical Considerations and Nomenclature for Reflectance. NBS monograph 160. U.S. Dept. of Commerce, National Bureau of Standards, Washington, D.C., 52 pp.

Raynolds, M.K., Walker, D.A., Munger, C.A., Vonlanthen, C.M., Kade, A.N., 2008. A map analysis of patterned-ground along a North American Arctic Transect. J. Geophys. Res 113 (G03S03).

Stuffler, T., Kaufmann, C., Hofer, S., Förster, K.P., Schreier, G., Mueller, A., Eckardt, A., Bach, H., Penné, B., Benz, U., Haydn, R., 2007. The EnMAP hyperspectral imager--An advanced optical payload for future applications in Earth observation programmes: Bringing Space Closer to People, Selected Proceedings of the 57th IAF Congress, Valencia, Spain, 2-6 October, 2006. Acta Astronautica 61 (1-6), 115–120.

Vierling et. al. (1997): Differences in arctic tundra vegetation type and phenology as seen using bidirectional radiometry in the early growing season. In: Remote Sensing of Environment, Jg. 60, H. 1, S. 71–82. doi.org/10.1016/S0034-4257(96)00139-3.

Vonlanthen, C.M., Walker, D.A., Raynolds, M.K., Kade, A., Kuss, P., Daniëls, F.J.A., Matveyeva, N.V., 2008. Patterned-Ground Plant Communities along a bioclimate gradient in the High Arctic, Canada. Phytocoenologia 38 (1), 23–63.

Walker, D.A., Epstein, H.E., Welker, J.M., 2008a. Introduction to special section on Biocomplexity of Arctic Tundra Ecosystems. J. Geophys. Res 113 (G3).

Walker, D.A., Kuss, P., Epstein, H.E., Kade, A.N., Vonlanthen, C.M., Raynolds, M.K., Daniëls, F.J., 2011. Vegetation of zonal patterned-ground ecosystems along the North America Arctic bioclimate gradient. Applied Vegetation Science 14 (4), 440–463

Walker, D.A., Raynolds, M.K., Daniëls, F.J.A., Einarsson, E., Elvebakk, A., Gould, W.A., Katenin, A.E., Kholod, S.S., Markon, C.J., Melnikov, E.S., Moskalenko, N.G., Talbot, S.S., Yurtsev, B.A., The other members of the CAVM Team, 2005. The Circumpolar Arctic vegetation map. Journal of Vegetation Science 16 (3), 267–282.

Appendix

A.1. Detailed Field Work Overview

Tab. A.1.1: *field activity codes*

Code	Field activity	Description
00	Site description	Vegetation description (Braun-Blanquet, vegetation height); soil moisture measurements; site description (slope, weather); Munsell colour description of the plant species; GPS coordinates
01	Overview photos	overview images from all four cardinal points
02	Grid plot photos	Detailed photos of all 100 plots within one 10x10 m grid (study site)
03	panorama photos	360° panorama photos in visible and near-infrared
04	spectrometry	Spectro-radiometric measurement of all 100 plots withing one 10x10 m grid (study site)
05	BRDF	BRDF measurements with the ManTIS spectro-goniometer (number in brackets shows the amount of full spherical measurements at various sun zenith angles)

Tab. A.1.2: *conducted field work during the EyeSight-NAAT-ALASKA 2012 expedition*

Site ID	Field Activity Code	Date	Comments
HV_footslope	00	2012-06-26	
	01	2012-06-26	
	02	2012-06-27	
	03	2012-07-02	
	04	2012-06-27	Spectrometry under clouded conditions
	04	2012-06-29	Spectrometry under clear sky
HV_midslope	00	2012-06-26	
	01	2012-06-26	
	02	2012-06-27	
	03	2012-07-02	
	04	2012-06-27	Spectrometry under clouded conditions
	04	2012-06-29	Spectrometry under clear sky
HV_hillcrest	00	2012-06-26	
	01	2012-06-26	
	02	2012-06-27	
	03	2012-07-02	
	04	2012-06-27	Spectrometry under clouded conditions
	04	2012-06-29	Spectrometry under clear sky
	05 (4)	2012-06-30	BRDF measurement of a tussock at four sun zenith angles
	05 (4)	2012-07-02	BRDF measurement of an area between two tussocks at four sun zenith angles
SW_MAT	00	2012-07-04	
	01	2012-07-04	
	02	2012-07-04	
	03	2012-07-04	
	04	2012-07-04	
SW_MNT	00	2012-07-04	
	01	2012-07-04	
	02	2012-07-04	
	03	2012-07-04	
	04	2012-07-04	
FB_wet	00	2012-07-06	
	01	2012-07-06	

	02	2012-07-10	
	03	2012-07-07	
	04	2012-07-09	Measurement aborted due to cloud cover
	04	2012-07-10	
FB_zonal	00	2012-07-06	
	01	2012-07-06	
	02	2012-07-09	
	03	2012-07-07	
	04	2012-07-09	
	05 (6)	2012-07-07	BRDF measurement of a sedge plot at six sun zenith angles
	05 (3)	2012-07-09	BRDF measurement of a salix plot at three sun zenith angles
	05 (1)	2012-07-13	BRDF measurement of a frost boil at one sun zenith angles
	05 (3)	2012-07-15	BRDF measurement of a horsetail plot at three sun zenith angles
FB_dry	00	2012-07-06	
	01	2012-07-06	
	02	2012-07-09	
	03	2012-07-07	
	04	2012-07-09	
DH_zonal	00	2012-07-11	
	01	2012-07-11	
	02	2012-07-11	
	03	2012-07-11	
	04	2012-07-11	

A.2. Overview of the spectral reflectance data of the nine study sites

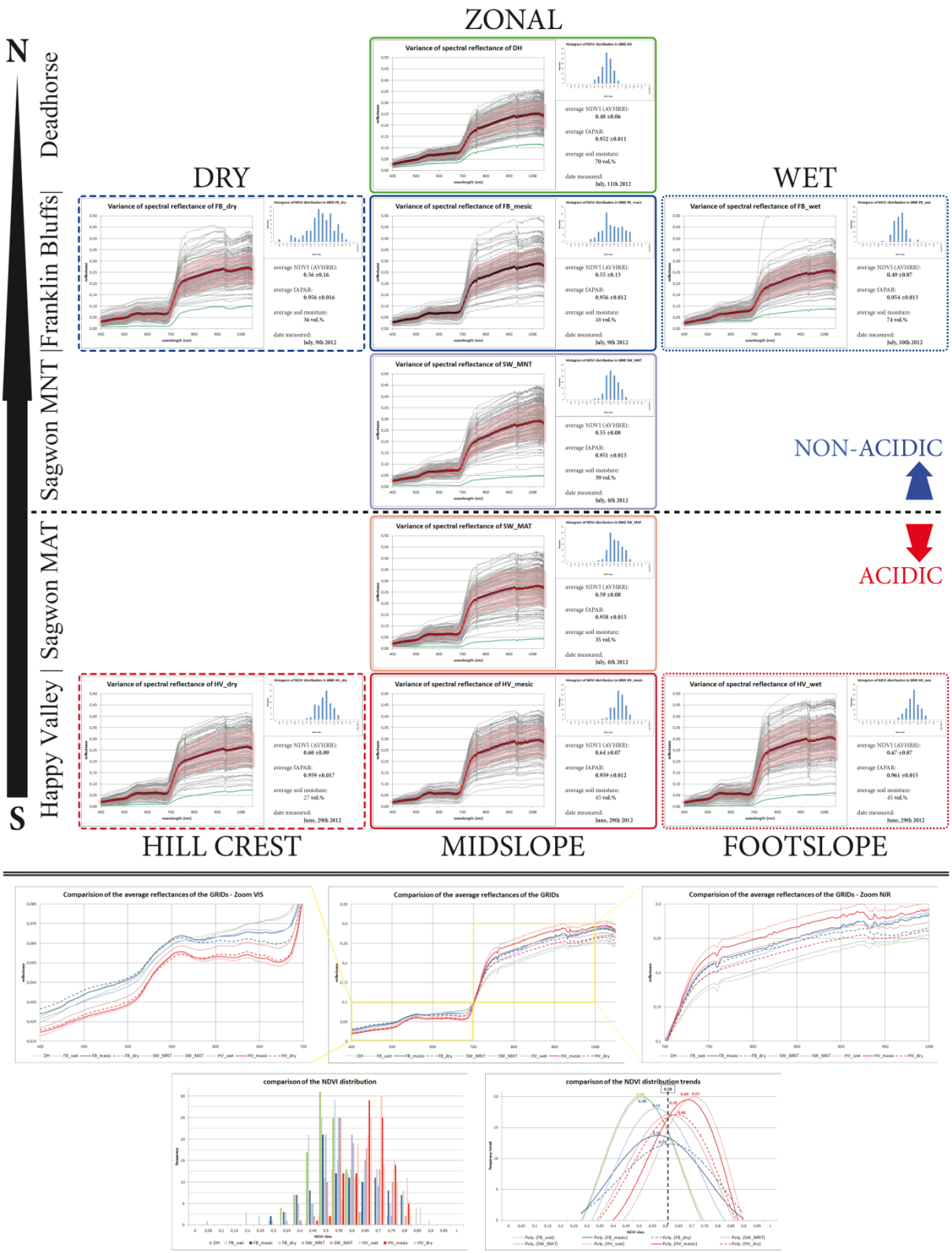

A.3. Overview of the NDVI data of the nine study sites

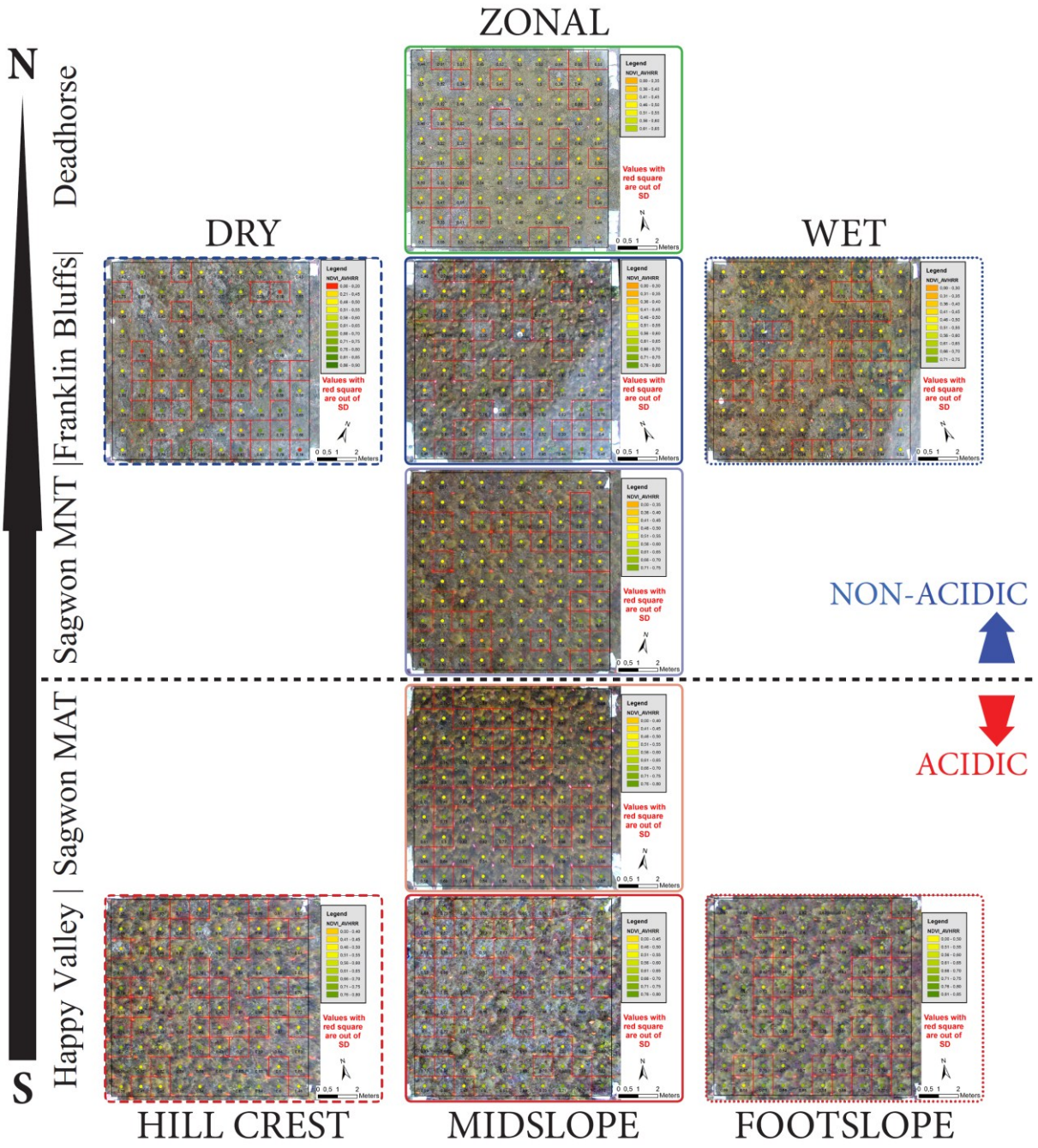

Die "Berichte zur Polar- und Meeresforschung" (ISSN 1866-3192) werden beginnend mit dem Heft Nr. 569 (2008) als Open-Access-Publikation herausgegeben. Ein Verzeichnis aller Hefte einschließlich der Druckausgaben (Heft 377-568) sowie der früheren **"Berichte zur Polarforschung"** (Heft 1-376, von 1981 bis 2000) befindet sich im open access institutional repository for publications and presentations (**ePIC**) des AWI unter der URL http://epic.awi.de. Durch Auswahl "Reports on Polar- and Marine Research" (via "browse"/"type") wird eine Liste der Publikationen sortiert nach Heftnummer innerhalb der absteigenden chronologischen Reihenfolge der Jahrgänge erzeugt.

To generate a list of all Reports past issues, use the following URL: http://epic.awi.de and select "browse"/"type" to browse "Reports on Polar and Marine Research". A chronological list in declining order, issues chronological, will be produced, and pdf-icons shown for open access download.

Verzeichnis der zuletzt erschienenen Hefte:

Heft-Nr. 643/2012 — "The Expedition of the Research Vessel 'Sonne' to the subpolar North Pacific and the Bering Sea in 2009 (SO202-INOPEX)", edited by Rainer Gersonde

Heft-Nr. 644/2012 — "The Expedition of the Research Vessel 'Polarstern' to the Antarctic in 2011 (ANT-XXVII/3)", edited by Rainer Knust, Dieter Gerdes and Katja Mintenbeck

Heft-Nr. 645/2012 — "The Expedition of the Research Vessel 'Polarstern' to the Arctic in 2011 (ARK-XXVI/2)", edited by Michael Klages

Heft-Nr. 646/2012 — "The Expedition of the Research Vessel 'Polarstern' to the Antarctic in 2011/12 (ANT-XXVIII/2)", edited by Gerhard Kattner

Heft-Nr. 647/2012 — "The Expedition of the Research Vessel 'Polarstern' to the Arctic in 2011 (ARK-XXVI/1)", edited by Agnieszka Beszczynska-Möller

Heft-Nr. 648/2012 — "Interannual and decadal variability of sea ice drift, concentration and thickness in the Weddell Sea", by Sandra Schwegmann

Heft-Nr. 649/2012 — "The Expedition of the Research Vessel 'Polarstern' to the Arctic in 2011 (ARK-XXVI/3 - TransArc)", edited by Ursula Schauer

Heft-Nr. 650/2012 — "Combining stationary Ocean Models and mean dynamic Topography Data", by Grit Freiwald

Heft-Nr. 651/2012 — "Phlorotannins as UV-protective substances in early developmental stages of brown algae", by Franciska S. Steinhoff

Heft-Nr. 652/2012 — "The Expedition of the Research Vessel 'Polarstern' to the Antarctic in 2012 (ANT-XXVIII/4)", edited by Magnus Lucassen

Heft-Nr. 653/2012 — "Joint Russian-German Polygon Project East Siberia 2011 - 2014: The expedition Kytalyk 2011", edited by Lutz Schirrmeister, Lyudmila Pestryakova, Sebastian Wetterich and Vladimir Tumskoy

Heft-Nr. 654/2012 — "The Expedition of the Research Vessel 'Polarstern' to the Antarctic in 2012 (ANT-XXVIII/5)", edited by Karl Bumke

Heft-Nr. 655/2012 — "Expeditions to Permafrost 2012: 'Alaskan North Slope / Itkillik', 'Thermokarst in Central Yakutia' and 'EyeSight-NAAT-Alaska', edited by Jens Strauss, Mathias Ulrich and Marcel Buchhorn